Technical Letter Report on Evaluation of Time-Dependent Leak Rates in Alloy 600 Steam Generator Tube Specimens

August 31, 2010

Prepared by
C. B. Bahn and S. Majumdar
Argonne National Laboratory
Lemont, Illinois 60439

NRC Contract # JCN-N6582
Program Manager: Charles Harris

Table of Contents

Executive Summary

Primary-to-secondary leakage in pressurized water reactor units is limited, in part, to ensure that the offsite radiological consequences and control room operator doses remain within applicable limits. As a result it is important to be able to quantify the rate of primary-to-secondary leakage under various conditions, including design basis accidents. Historically, it has been assumed that the primary-to-secondary leak rate remains constant under a specific set of loading conditions. Recent test results have drawn into question the conservatism of this assumption. This report evaluates prior testing and analysis that was performed to assess whether the primary-to-secondary leak rate is time dependent (i.e., increases under constant loading condition) and identifies additional research that may be useful in further understanding of this phenomenon.

Argonne National Laboratory (ANL) has performed several series of leak rate tests of steam generator (SG) tubing that contains stress corrosion cracks. In some cases, dramatic increases in leak rates have been observed over relatively short times under nominally constant pressure conditions. The Electric Power Research Institute (EPRI) implemented a program to determine the significance of this ANL leak rate test data relative to the leakage integrity of operating SGs and the current industry methodologies of determining, evaluating, and projecting the leak integrity of service-degraded SG tubing.

ANL stress corrosion cracking (SCC) and electro-discharged machining (EDM) notch tube specimens that have shown time-dependent leak rate behaviors under constant pressure were characterized by fractography to determine the time-dependent crack growth mechanism. While some specimens showed typical ductile fracture surface features, others showed distinct crystallographic facets typical of fatigue crack growth at low ΔK level. This imp lies that time-dependent leak rate growth cannot be attributed to a single mechanism.

Some SCC specimens which were fabricated using a high-pressure pump, and trapezoidal EDM notch specimens, fabricated with and without a high-pressure pump, indicated fatigue crack growth on their fracture surfaces. Structural vibration, which is very likely the underlying cause for the observed fatigue, appears to be the result of the pressure oscillation induced by the high-pressure pump and interaction between the water jet and the tube structure. The pressure oscillation amplitude and frequency induced by the high-pressure pump could be estimated from the power spectral density analysis for the pressure transducer signals, which corresponded to the frequency of the pump piston stroke. The water-jet-induced pressure oscillation could not be estimated from the measured data but had to be estimated from modeling and earlier literature. There are two possible water-jet-induced vibration phenomena: jet vortex shedding at the jet nozzle exit and cavitation-induced vibration at the jet nozzle inlet. For stress corrosion cracks in SG tubing, both sources may contribute to fatigue crack growth of the SG tubing.

Crack growth analyses of the specimens with trapezoidal and rectangular EDM notch specimens have indicated that both the high-pressure pump and the water jet could significantly contribute to fatigue crack growth. Although our primary purpose is to determine the critical conditions under which the water jet significantly affects the fatigue crack growth, the pressure oscillations of the high-pressure pump tend to obscure the jet effect. Pump pressure oscillation effects can be eliminated by conducting the leak rate tests under constant pressure in the high-pressure blowdown facility, which because of the absence of a pump can provide a steady supply of water under constant pressure.

After detailed analyses of the ANL leak rate tests and review of earlier literature, we have developed an experimental plan has been developed as follows: Currently available fatigue crack growth rate equation of alloy 600 has significant uncertainty in the lower stress intensity range and higher load ratio because the available experimental data are limited. To validate the fatigue crack growth rate equation, and to evaluate the crack growth by jet/structure

interaction, fatigue tests that can determine the fatigue threshold as a function of load ratio are necessary. Leak rate tests at constant pressure are needed to determine the critical condition under which the water jet effect becomes significant within 24 hours as a function of crack length. Since earlier tests have shown that an impinging water jet tends to increase the crack growth rate compared to that under a free jet, we propose to surround the test tube specimen with a simulated neighboring SG tube bundle. To measure the jet induced vibration frequencies in situ, accelerometers or an ultra-high-speed camera can be placed in close proximity to the crack.

Using the approach described above, ANL should be able to clarify experimental questions, and provide recommendations for suitable future procedures to ensure the validity of industry's primary-to-secondary leakage assessments and predictions.

Introduction

Under sponsorship of the U.S. Nuclear Regulatory Commission (NRC), Argonne National Laboratory (ANL) has performed several series of leak rate tests on steam generator (SG) tubing containing laboratory grown stress corrosion cracking (SCC). Prior test results have been published.[1] In some cases, dramatic increases in leak rates have been observed over relatively short times under nominally constant pressure conditions (nominally 17.3 MPa (2500 psig)). A series of tests conducted on specimens with trapezoidal electro-discharged machining (EDM) notches (outside diameter [OD] length shorter than inside diameter [ID] length) also showed such behavior.[2] Post-test visual examination clearly revealed that the OD crack length of these EDM specimens had increased through tearing of the tapered ligaments ahead of the notch tips. Specimens with rectangular through-wall (TW) EDM notches (10-15 mm [0.4-0.6 in.] length) also showed a time-dependent increase in leak rate under constant pressure (9.1-12 MPa [1300-1700 psig]) hold (with an active water jet) and post-test visual examination showed clear evidence of notch tip tearing through full-thickness material.[2] Hwang et al.[3,4] reported a time-dependent increase in leak rates of Alloy 600 tubing at constant pressure. They used a similar test system to that in the ANL leak rate tests, but they did not hold the pressure constant for more than one hour.

At one nuclear power plant, a SG tube was tested in-situ to obtain the burst pressure and leakage potential for a crack-like indication. The results showed that the leak rate increased for 1-2 min during the test period at constant pressure. The results from this test are not directly applicable to those observed in the ANL leak rate tests because the test pressure was higher (approx. 4,000 psig) and the hold time at constant pressures was much shorter than those in the ANL tests.

Such time-dependent leak rate increases suggest that the time-dependent crack growth can occur at room temperature in Alloy 600 tube specimens tested with relatively non-corrosive water (tap water). The number of possible mechanisms for time-dependent crack growth at room temperature and constant pressure is likely limited. Because tap water was used and leak rate growth was observed even at room temperature, corrosion-related mechanisms such as SCC or hydrogen embrittlement are unlikely. Type 304 stainless steel has been reported to exhibit creep at room-temperature.[5] Therefore, an expectation that Alloy 600 tubing materials can creep at room temperature is not unreasonable, particularly if the stress level is extremely high, i.e., close to ultimate tensile strength. For these reasons, time-dependent ductile tearing by creep has been suggested as a possible mechanism for the observed crack growth. The other possible mechanism is fatigue. Once the SCC crack grows sufficiently in length, the leaking water from the crack becomes a jet with entrained water droplets, which may cause a water jet/structure interaction that can induce high-frequency vibratory loading. Of the two, fatigue is the likelier cause because tests using a static head for pressurization of a specimen in which the jet was suppressed by inserting a bladder in the specimen did not reveal any increase of notch length after 24 h of testing. Fractography observations of ANL leak rate test specimens could be used to determine whether fatigue or ductile tearing by creep was responsible for the observed time-dependent crack growth.

The Electric Power Research Institute (EPRI) has implemented a program to determine the significance of the ANL leak rate test data relative to the leakage integrity of operating SGs and the current methodologies of determining, evaluating, and projecting the leak integrity of service-degraded SG tubing. Phase 1 of the EPRI program involved a full characterization of the ANL leak rate test results, including fractography of the test specimens. The results have been published in detail elsewhere.[6] In the current report, results from the EPRI program are evaluated and reviewed together with other available literature, and a possible future work plan is proposed on the basis of that evaluation.

Characterization of ANL Leak Rate Specimens

Characterization Results

A list of the SCC specimens used in prior ANL constant-pressure leak rate tests was prepared. The leak rate data as a function of time for available specimens were reviewed and the specimens that showed a time-dependent leak rate increase were selected for further characterization. The fractography of the selected specimens was characterized by scanning electron microscopy (SEM). One of the objectives of the EPRI program was to determine if the ANL SCC specimens have an unusually (uncharacteristic) high degree of intergranular attack (IGA), which could potentially lead to time-dependent cracking and thus explain the observed time-dependent increase of leak rate. To evaluate the degree of IGA, radial metallography was also used.

Table 1 shows a list of ANL SCC leak rate test specimens that were tested as part of the NRC-sponsored SG tube integrity program (ISG-TIP-2 and ISG-TIP-3) at ANL. Two test facilities were used for the leak rate tests; one is the "blowdown test facility" and the other is the "room-temperature high -pressure test facility," both of which have been described in an earlier report.[1] The shaded specimens in Table 1 were selected for further characterization. A total of eight SCC specimens was selected. All but one of the SCC specimens were made by ANL using sodium tetrathionate solution at room temperature and internal pressurization. The one exception was Specimen W-2-10, which was made by Westinghouse via a doped-steam method. One EDM-notched specimen (Specimen ID: NUANOD.2D) was also characterized so that it was compared with the SCC specimens. Thus, a total of nine leak rate test specimens was characterized under the EPRI program (Phase 1).

In this report, three representative SCC specimens and one EDM notch specimens were selected for review: W-2-10, SGL-822, SGL-900, and NUANOD.2D. W-2-10 was selected because of the different SCC specimen fabrication method (doped steam vs. chemicals at room temperature), and SGL-822 and SGL-900 were selected because they are representative specimens showing fractographic indications of ductile tearing and fatigue, respectively. The EDM-notched specimen NUANOD.2D was selected to compare its fractographic result with those of SCC specimens. An additional EDM-notched specimen NUANOD.2-1.0 was characterized and compared with the other specimens. NUANOD.2-1.0 was selected because it showed evidence of fatigue fracture even though it was tested in the blowdown test facility. Detail results of each specimen are reviewed in the following section.

Table 1. ANL SCC leak rate test specimens [Reprinted with permission from EPRI].[6]

Tube Desig-nation	SCC Fabricator	Heat #	Tube Available ?	Leak Test @RT ?[1]	Time-Dependent Leak Rate @RT ?	Leak Test @HT ?[1]	Time-Dependent Leak Rate @HT ?	Crack Opened ?	ANL Heat Treatment	Comment
SGL-177	ANL[2]	NX8527	Yes	Yes	Yes	No	No	Yes	10 min @1100 C, 48 hr @600 C	
SGL-195	ANL	NX8527	No[4]	Yes	No	No	No	Yes	10 min @1100 C, 48 hr @600 C	
SGL-104	ANL	NX8527	Yes	No	No	Yes	No	Yes	10 min @1100 C, 48 hr @600 C	
SGL-219	ANL	NX8527	Yes	No	No	Yes	Yes	Yes	10 min @1100 C, 48 hr @600 C	Only half of crack surface is available
W-2-10	Westinghouse[3]		Yes	Yes	Yes	Yes	No	Yes		
SGL-731	ANL	NX8520HT	Yes	Yes	No	No	No	Yes	48 hr @600 C	
SGL-822	ANL	NX8520LT	Yes	No	No	Yes	Yes	Yes	48 hr @600 C	Dented
SGL-876	ANL	NX8520LT	Yes	Yes	No	Yes	No	Yes	48 hr @600 C	Unstable burst at high-temperature test
SGL-750	ANL	NX8520LT	Yes	Yes	Yes	Yes	No[6]	No	48 hr @600 C	
SGL-904	ANL	NX8520LT	Yes	Yes	Yes	Yes	No[6]	No	48 hr @600 C	
SGL-905	ANL	NX8520LT	Yes	Yes	Yes	Yes	No[6]	No	48 hr @600 C	
SGL-911	ANL	NX8520LT	Yes	Yes	Yes	Yes	No[6]	No	48 hr @600 C	Cracked near roll transition zone
SGL-900	ANL	NX8520LT	Yes	Yes	Yes	No	No	No	48 hr @600 C	
SGL-959	ANL		Yes	Yes	No	No	No	No	48 hr @600 C	Plugged by particles
SGL-968	ANL		Yes	Yes	No	No	No	No	48 hr @600 C	Pressurized to 1400 psi without leak
SGL-973	ANL		No[5]	Yes	Yes	No	No	Yes	48 hr @600 C	

1. All leak tests at high temperature were performed at the blowdown test facility. All leak tests at room temperature were performed at room-temperature high-pressure test facility, except specimens SGL-177, SGL-195, and W-2-10, which were tested at the blowdown test facility.
2. ANL made laboratory-grown SCC cracks by using sodium tetrathionate at room temperature.
3. Westinghouse made laboratory-grown SCC cracks by a doped steam method.
4. The tube was sectioned circumferentially and mounted for metallography.
5. The tube has been cut, but is missing.
6. The holding time at constant pressure and high temperature was too short (less than 15 minutes).

W-2-10

Specimen W-2-10 was made by Westinghouse with a doped-steam method and was tested in the blowdown test facility at room temperature and high pressure. Even though the increase in leak rate at constant pressure of ~18 MPa (2600 psig) and room temperature was observed, the leak rate itself was much lower than those of other specimens, i.e., less than 0.1 L/min (0.03 gpm).

Figure 1 is an SEM photographic montage of W-2-10. This specimen has a long non-SCC radial ligament and short radial ligaments located in the middle of a TW SCC zone. The short ligaments (with a radial depth of less than 50 μm) were located in the TW SCC zone and showed ductile fracture feature such as dimples and voids. These short ligaments may have fractured during pressurization or during the constant-pressure hold by creep; this caused a relatively small increase in time-dependent leak rate. Therefore, it is likely that the time-dependent increase in leak rate observed at ~18 MPa (2600 psig) was caused by ductile tearing of the short radial ligaments located in the middle of the TW SCC zone.

After the SEM fractography was performed, the specimen was mounted and polished for radial metallography. The specimen did not show significant secondary cracking or IGA along the dominant stress corrosion crack, except in one area where secondary cracking was significant. However, secondary cracking diminished gradually along the radial depth, which is reasonable because the dominant axial SCC began at the OD surface and propagated toward the ID surface.

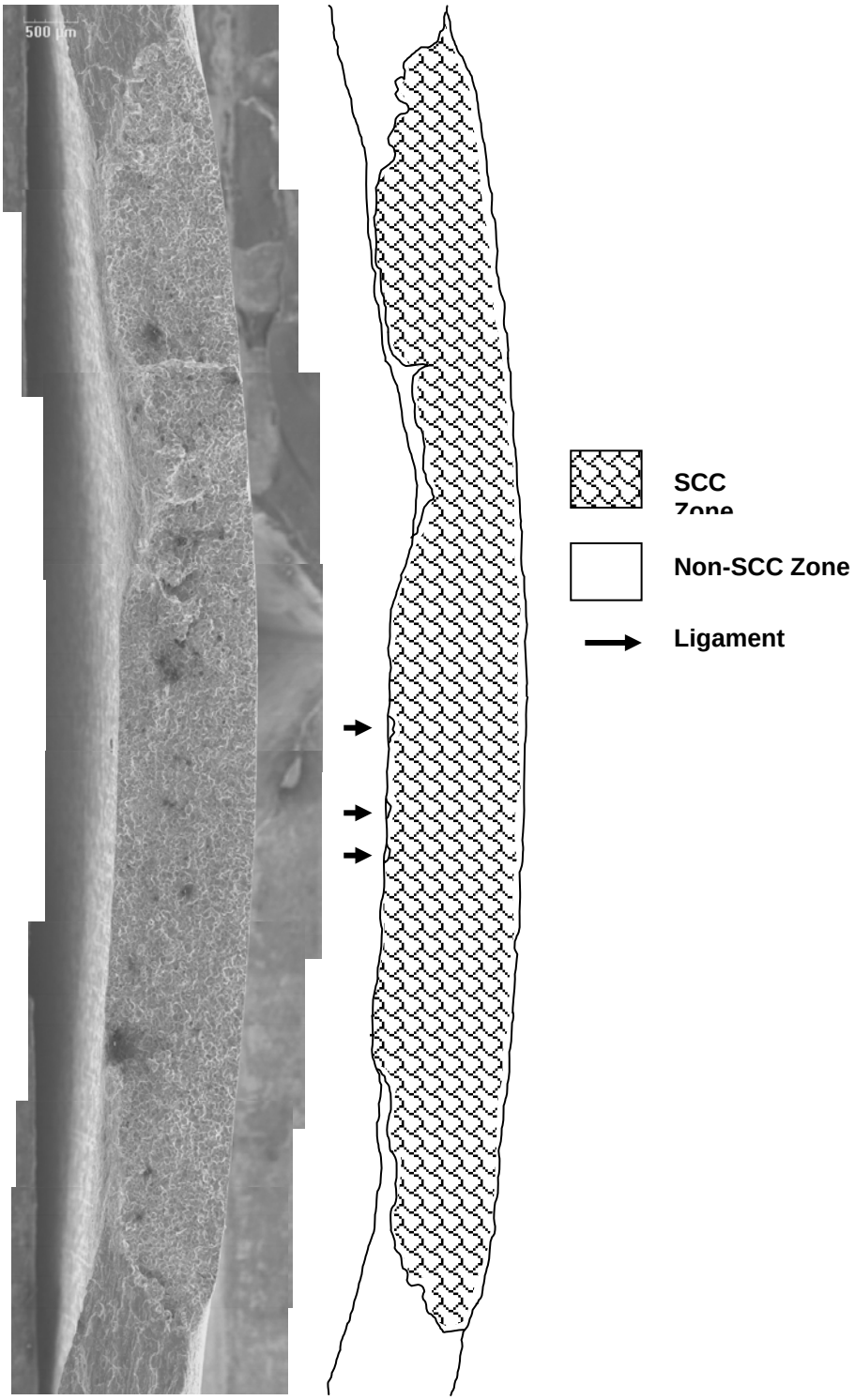

Figure 1. SEM fractograph of W-2-10 specimen; left edge is tube ID and right edge is tube OD (50X magnification) [Reprinted with permission from EPRI].[6]

SGL-822

Specimen SGL-822 was tested at 282°C (540°F) in the blowdown test facility. The leak rate stabilized after gradually increasing from 6 to 19 L/min (1.5 to 5 gpm @ 282°C) over 35 min. The initial leak rate was relatively high compared to that of other specimens, suggesting that this specimen had a longer TW SCC region.

Figure 2 is a SEM photographic montage of SGL-822. The specimen had two radial ligaments in the TW SCC region; one was relatively long and large (Ligament 1) and the other was short (Ligament 2). Figure 3, a high-magnification view of Ligament 1, shows three distinct regions: an SCC region, a stretch zone with slip offsets. and a typical ductile fracture zone with voids. The increase in leak rate of SGL-822 appears to be induced by ductile tearing of the two ligaments. Because the fractography suggested that the crack did not grow beyond the original SCC zone during the leak test, except for the two ligaments, it is likely that the remaining radial ligaments in the TW SCC zone were so long that their gradual tearing would have caused the significant increase in leak rate seen during the test. Fractographic results for W-2-10 and SGL-822 suggest that ductile tearing of the remaining radial ligaments located in the middle of the TW SCC zone, possibly by creep, was the cause of the time-dependent increase in leak rates regardless of the SCC specimen fabrication methods (doped steam vs. chemicals at room temperature).

Radial metallographic results along the dominant axial crack of SGL-822 are presented in Figure 4. The maximum IGA depth perpendicular to the main axial crack is about 500 μm near the OD surface, and the degree of IGA becomes less with depth but is still significant away from the OD surface. It is likely that the sodium tetrathionate solution used at ANL to produce the laboratory grown SCC specimens attacked grain boundaries near the dominant axial stress corrosion crack. This was confirmed by radial metallographic results of other SCC specimens. A remaining issue is whether this IGA affected the time-dependent increase in leak rates of SCC specimens. Because two specimens, one with IGA (SGL-822) and the other without significant IGA (W-2-10), showed similar fractographic results (i.e., ductile tearing of radial ligaments), it is not likely that the IGA had any effect on leak rate behavior of these two specimens. Also, this conclusion is supported by a comparison between SCC specimen SGL-900 and EDM-notched specimen NUANOD.2D and is discussed in later sections.

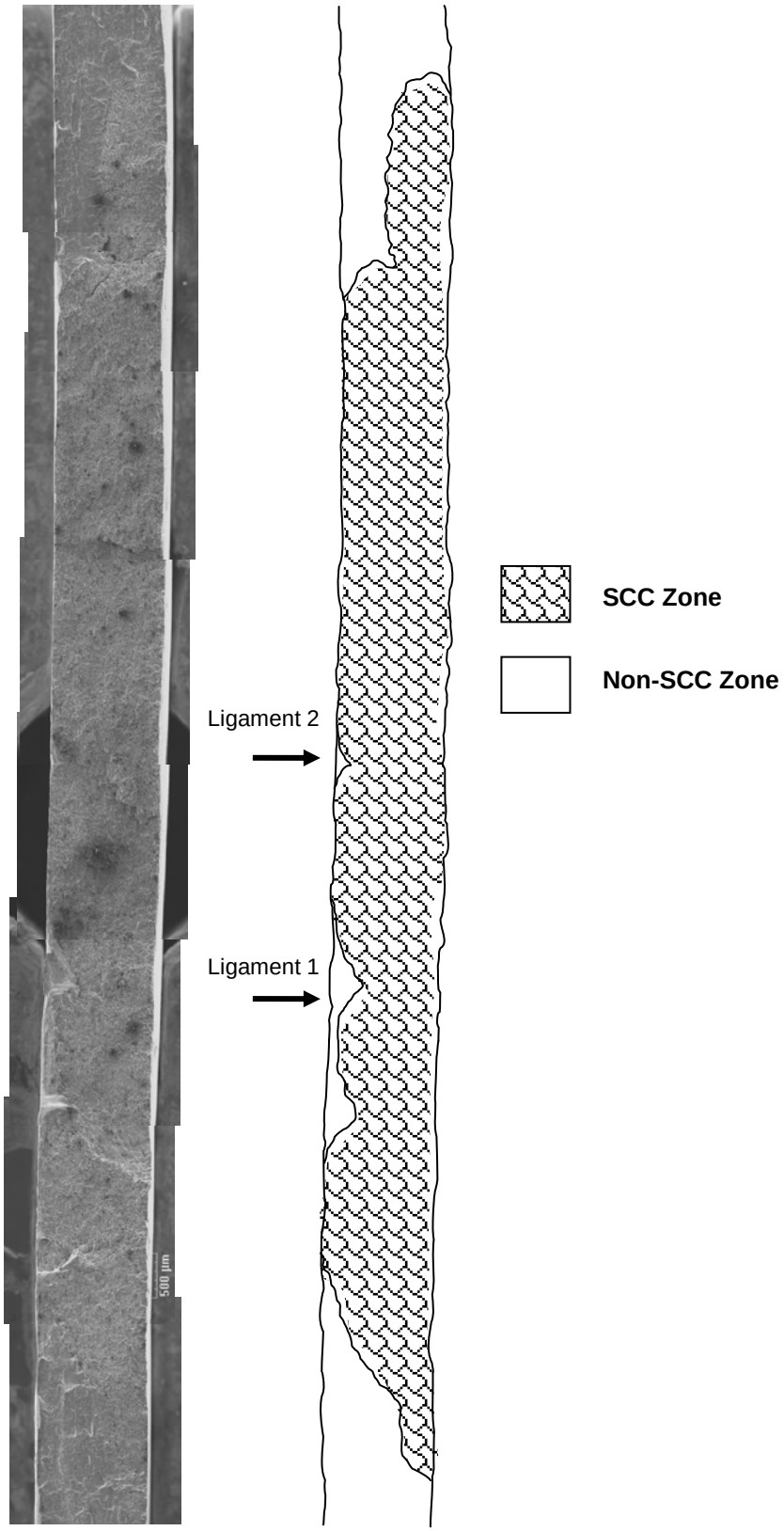

Figure 2. SEM fractograph for SGL-822 specimen; left edge is tube ID and right edge is tube OD (50X magnification) [Reprinted with permission from EPRI].[6]

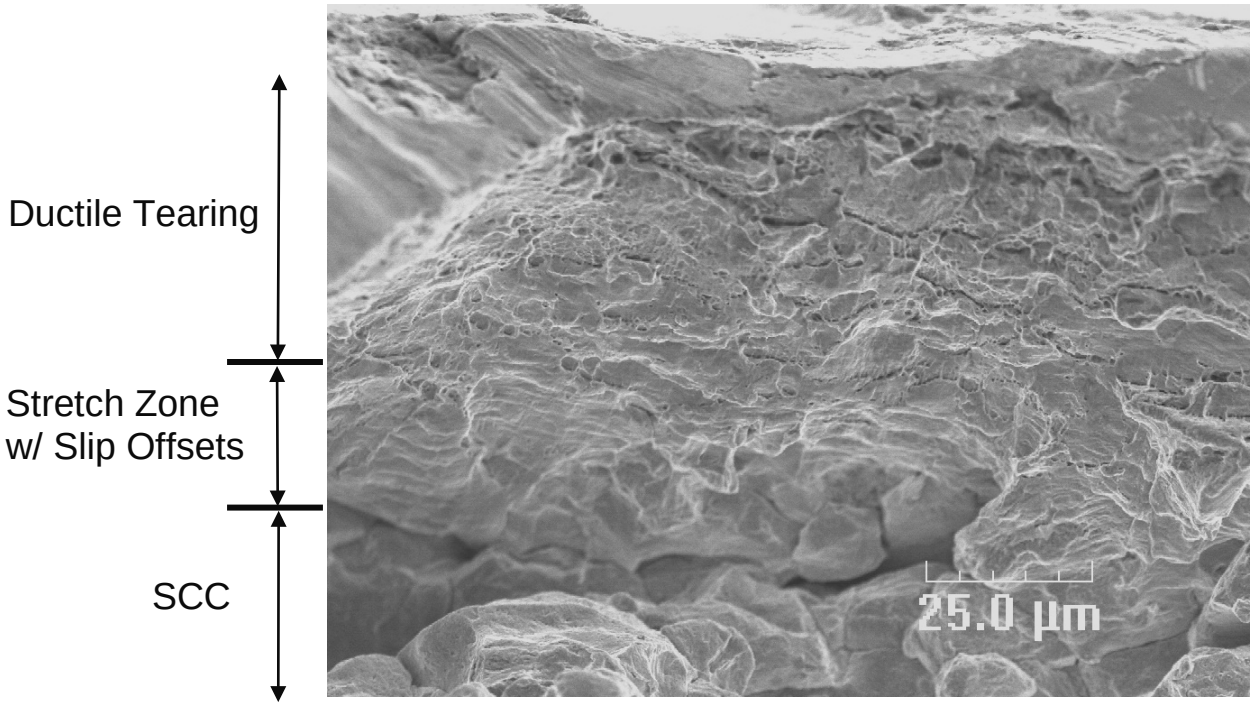

Figure 3. SEM fractograph for Ligament 1 region designated in Figure 2, showing three distinct regions: SCC region, stretch zone with slip offsets, and typical ductile fracture region with voids; top edge is tube ID [Reprinted with permission from EPRI].[6]

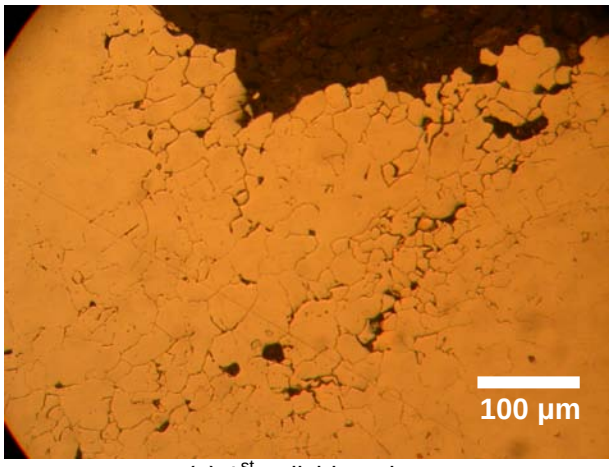

(a) 1st polishing plane

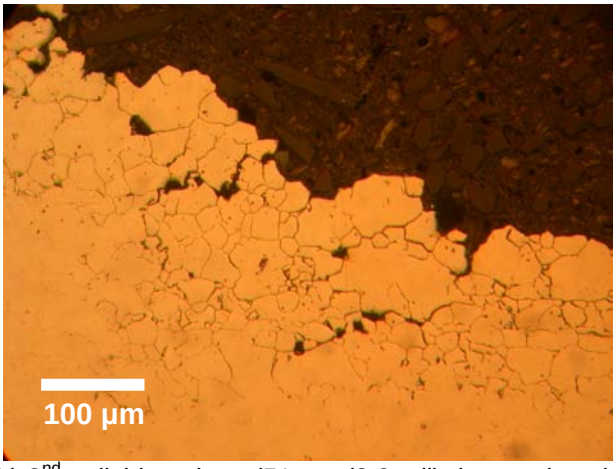

(b) 2nd polishing plane (51 µm (2.0 mil) deeper than (a))

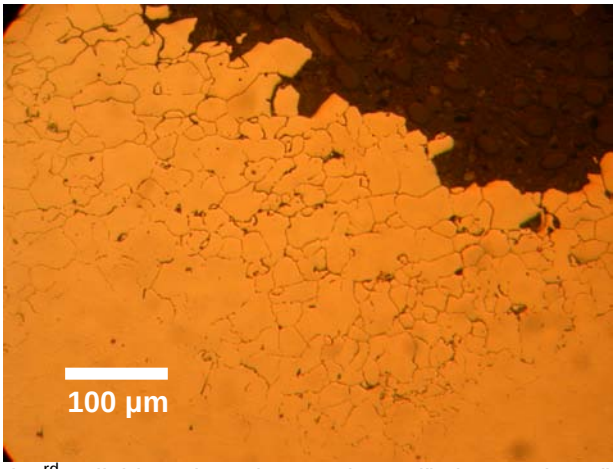

(c) 3rd polishing plane (25 µm (1.0 mil) deeper than (b))

Figure 4. Optical micrographs near the main axial crack of SGL-822 as a function of radial depth; upper edge is the main crack fracture surface [Reprinted with permission from EPRI].[6]

SGL-900

Five lab-grown axial ODSCC specimens (SGL-750, -900, -904, -905, and -911) that showed time-dependent increases in leak rates were tested in the room-temperature high-pressure test facility. This facility has a high-pressure pump that can continuously supply pressurized water up to a steady-state leak rate of 45 L/min (12 gpm). Because the fractographic and radial metallographic results, respectively, of the five specimens were similar, SGL-900 was selected as the representative one. The leak rate began at almost zero but gradually increased to >8 L/min (2 gpm) over a period of 9 hr.

Figure 5 is a montage of the overall fracture surface of SGL-900, showing an initial lab-grown SCC region, a region of crack growth during the leak test, and a final crack opening region after the leak test. This specimen had two ligaments in the middle of TW SCC zones. The ligament areas are larger than those of W-2-10 and are comparable with those of SGL-822. Some areas in these ligaments showed crystallographic facets and some areas appeared to show abrasion marks, but the fractographic features of neither could be clearly interpreted. Fractographic feature of ductile tearing was not observed in these ligaments. Figure 6 shows an SEM fractograph of the upper non-SCC region. It is noted that the initial stress corrosion crack grew axially beyond the original SCC length during the leak test, suggesting that a crack could grow in full-thickness material during the leak test. Figure 7 shows the SEM fractograph of the upper crack extension zone (non-SCC zone) away from the tip area, indicating crystallographic facets all over the fracture surface including the boundary between the SCC and the non-SCC zones. Figure 8 is a higher-magnification view of the region designated by the square in Figure 7 and clearly indicates the crystallographic facets. The fracture feature (crystallographic facets) observed in the ligaments and crack extension regions during the leak test is similar to those of the other four SCC specimens tested at room temperature.

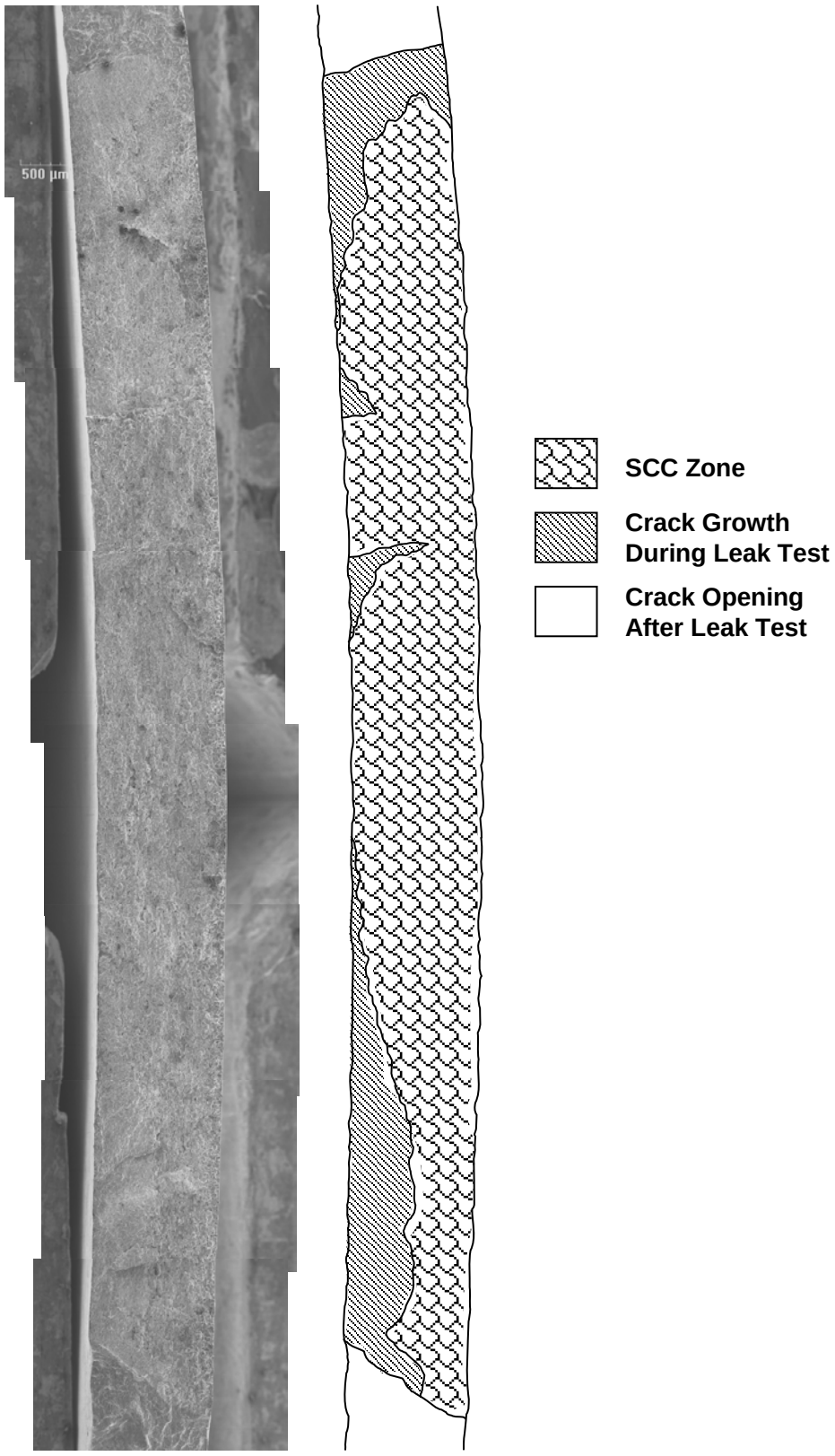

Figure 5. Montage for fracture surface of SGL-900 specimen; left edge is tube ID and right edge is tube OD (50X magnification) [Reprinted with permission from EPRI].[6]

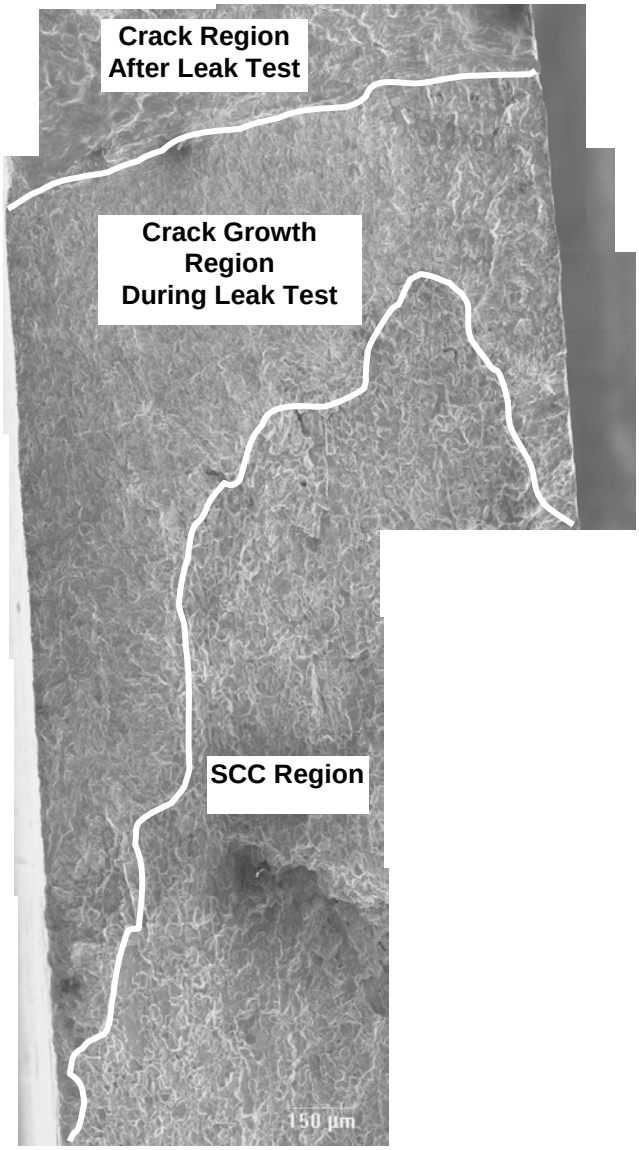

Figure 6. SEM fractograph showing three regions: SCC region, crack growth region during leak test, and crack region after leak test; indicating crack growth in full-thickness material during leak test [Reprinted with permission from EPRI].[6]

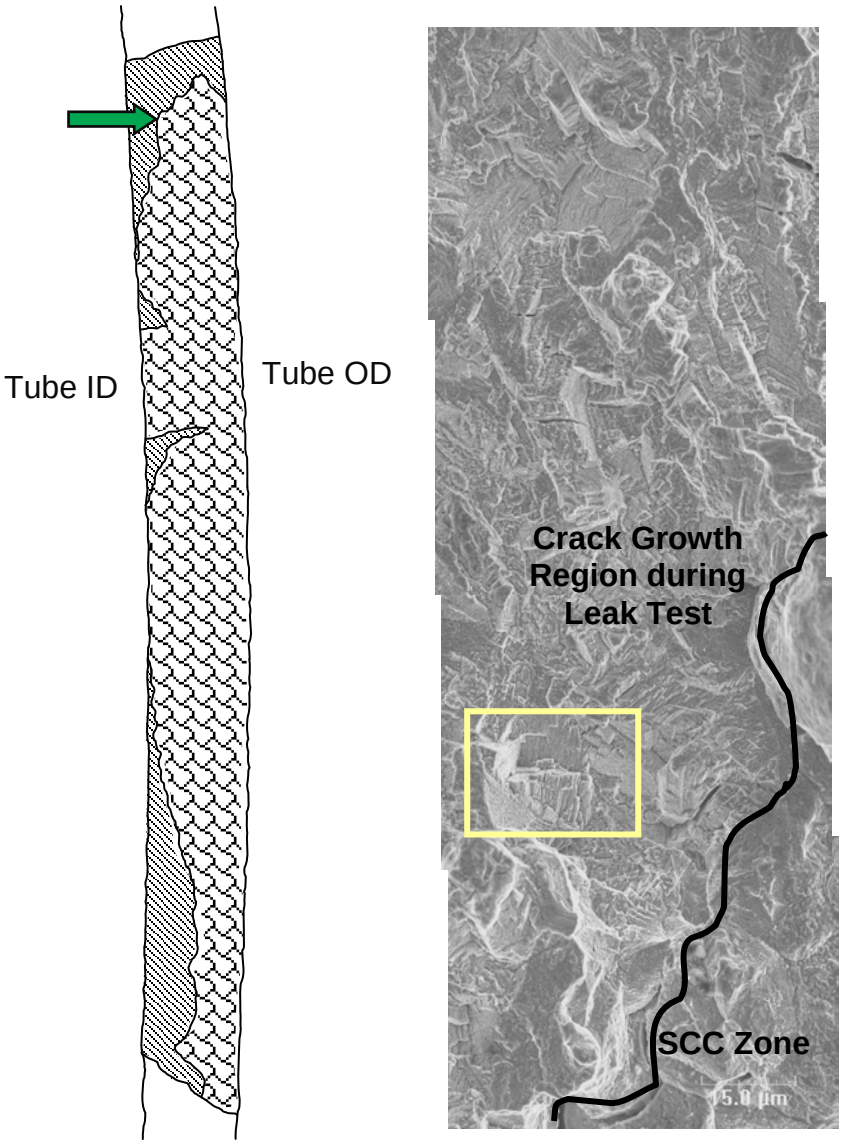

Figure 7. SEM fractograph for upper region of non-SCC zone designated by arrow in the left figure; bottom-right region is lab-grown SCC zone and the other region is the crack growth region during the leak test (2000X magnification) [Reprinted with permission from EPRI].[6]

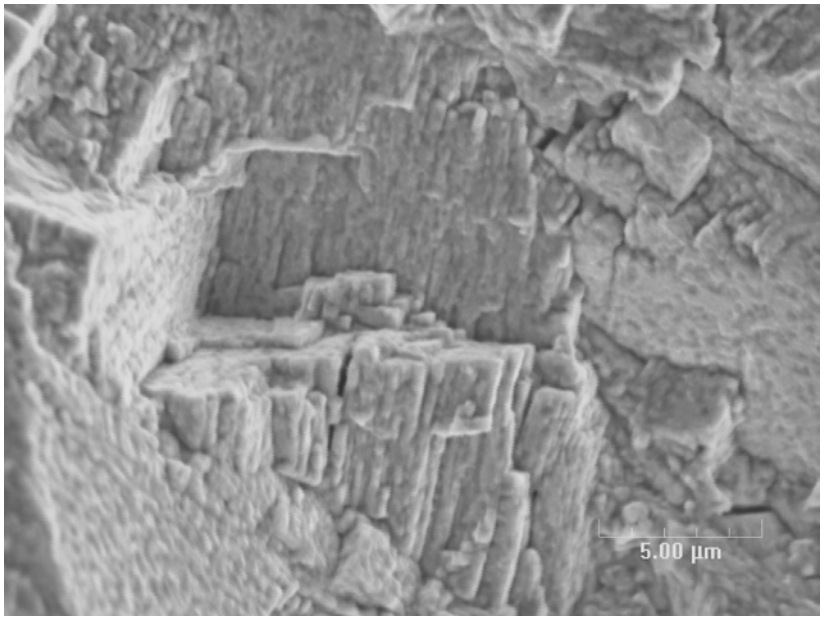

Figure 8. SEM fractograph for higher magnification of region designated by the box in Figure 7, indicating crystallographic facets (5000X magnification) [Reprinted with permission from EPRI].[6]

Initiation and initial propagation of a fatigue crack is defined as Stage I fatigue.[7] During Stage I, the fatigue crack tends to follow crystallographic planes but changes directions at discontinuities such as grain boundaries.[7] In general, Stage I fracture surfaces are angular with fairly smooth facets and do not exhibit fatigue striations. They are normally observed on high-cycle/low-ΔK fractures.[7] Mills and James discussed the fracture surface morphologies of Alloy 600 after fatigue testing in high-temperature water[8] or liquid sodium[9]. They showed that fatigue crack growth mechanisms were dependent on the prevailing stress intensity level. Striation formation was the dominant mechanism at ΔK levels above 20-25 MPa$\sqrt{m}$, and striation spacing generally agreed with macroscopic fatigue crack propagation rates at intermediate- and high-ΔK levels. Below 20 MPa$\sqrt{m}$, the dominant feature was crystallographic faceting, associated with a planar slip mechanism.[8] Because James and Mills[10] reported that Alloy 718 also showed the same dependency of fracture surface morphologies on stress intensity level after room-temperature fatigue tests, the effect of ΔK level on fatigue fracture surfaces of Alloy 600 at room temperature is expected to be similar to that in high-temperature water. Published fractography results of Alloy 600 tested near fatigue threshold at room temperature have shown crystallographic facets.[11] The fracture surface in that literature is similar to those of SGL-900 and Alloy 600 in high-temperature water reported by Milles and James. As shown in Figure 9, the fractographic results for Ni-base superalloy[12] fatigue tests near threshold are also similar to the fracture surfaces of SGL-900 shown in Figures 7-8. Therefore, fractographic results of SGL-900 suggest that the two large ligaments located in the TW SCC zone were fractured by fatigue at lowΔK level and the crack grew beyond the original SCC length, also by a fatigue mechanism. It is suggested that the crack grew by fatigue mechanism from the early stage of the leak test because the crystallographic facets were observed from the boundary between SCC zones and non-SCC zones. The leak rate data suggest that fatigue crack growth could potentially occur at relatively low leak rates (less than 8 L/min [2 gpm]).

Radial metallographic results indicated that, as was observed in Specimen SGL-822, the Specimen SGL-900 also had significant IGA along the dominant OD axial stress corrosion crack. The other four SCC specimens tested at room temperature also showed similar IGA along the dominant axial crack. The possible effect of IGA on the leak behavior of SCC specimens is discussed in a following section.

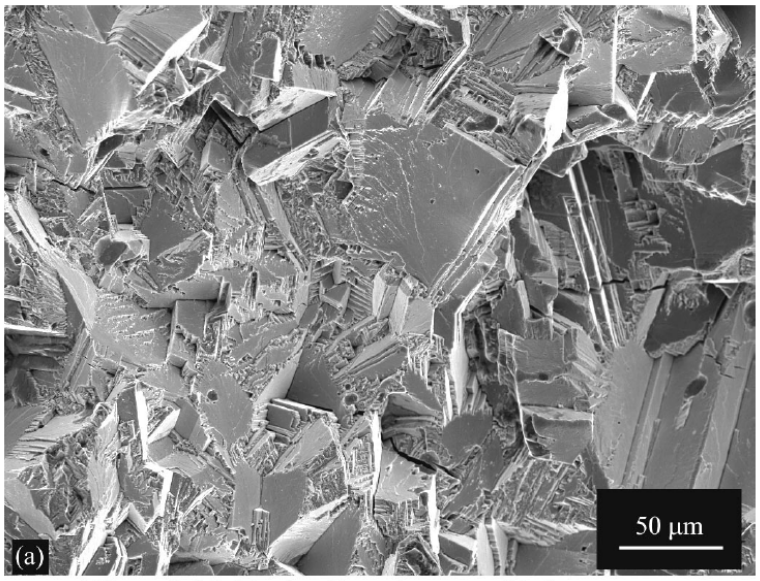

ΔK_o = 6.0 MPa√m, Roughness = 31.0 μm

Figure 9.
SEM fractograph of Ni-base superalloy showing near-threshold fracture surfaces at 1 kHz and R = 0.7 at room temperature [Reprinted with permission from TMS].[12]

NUANOD.2D

As a reference for comparison with SCC specimens, EDM-notched specimen NUANOD.2D was characterized. The initial notch length at the ID side was nominally 25 mm (1.0 in.) and that at the OD side was 5.1 mm (0.2 in.). To facilitate the visual observation of the crack growth intermittently, OD crack length was purposely machined to be shorter than ID crack length. The specimen was tested at 7 MPa (1000 psig) in the room-temperature high-pressure test facility. Because the crack opening area of an EDM-notched specimen is much larger than that of a SCC specimen of comparable length, the initial leakage level is much higher than that observed in SCC specimens. The leak rate increased from 6.1 to 17 L/min (1.6 to 4.5 gpm) during the test time of 700 min.

Fractographic results indicated crystallographic facets, which are indicative of fatigue crack growth at low ΔK level, as discussed earlier. Even though the crystallographic facets of NUANOD.2D are not as clear as those of SGL-900 (presumably because of the higher ΔK level than that of SGL-900), the fractographic result clearly indicates fatigue crack propagation. Therefore, it is concluded that the time-dependent increase in leak rates of NUANOD.2D was caused by fatigue crack growth.

The EDM-notched specimen does not have IGA along the main axial notch. But it showed fatigue fracture similar to SGL-900, which suggests that the presence of significant IGA along the main axial crack observed in SGL-900 did not affect the time-dependent increase in leak rates. The main cause of the time-dependent increase in leak rate is likely to be fatigue crack growth.

NUANOD.2-1.0

Two specimens (W-2-10 and SGL-822) tested earlier in the high-temperature blowdown test facility did not show any fatigue feature. Therefore, one might argue that the fatigue fracture observed on the specimens tested in the room-temperature high-pressure facility was caused solely by the difference in test facilities. A major difference between two test facilities is the high-pressure pump used in the room-temperature high-pressure facility, which causes significant pressure pulsation and possibly fatigue. Therefore, fatigue crack growth would not occur under a constant pressure condition like that in the blowdown test facility unless there is a fatigue source other than the pump. To prove that fatigue fracture by jet/structure interaction is possible under a constant pressure condition, the trapezoidal EDM-notch specimen NUANOD.2-1.0 was further characterized under the NRC Tube Integrity Program-4.

NUANOD.2-1.0 was 4.34 mm (0.171 in.) long at the OD and about 30.5 mm (1.2 in.) long at the ID. The specimen was tested in three stages to accumulate sufficient time for tearing with a primary water temperature of 316°C (600°F), which corresponds to a saturation pressure of 10.64 MPa (1543 psia)) and with a nitrogen gas cover pressure of 12.4 MPa (1800 psig). The secondary pressure on the outside of the flawed tube was controlled with a back-pressure valve operating on the steam discharge from the surrounding test module resulting from flashing of the leak flow. The secondary pressure was set at nominally 3.4 MPa (500 psig), which yielded the desired pressure difference across the tube of nominally 9.0 MPa (1300 psig).

Because of the limited water inventory of the blowdown vessel and the high leak rates of this EDM specimen, the maximum run time was 1 hr. To accumulate longer test times, the blowdown vessel was refilled and the test was repeated two more times to obtain a total of 170 min at the desired conditions. The first two tests were 1 hr each, and the third test, because of increased leak rate, was only 50 min long. The pressure differentials across the flaw for each test segment were 8.98, 9.76, and 9.65 MPa (1302, 1416, and 1399 psig), respectively, and the corresponding leak rates at the end of each test interval were 7.6, 9.5, and 12 L/min @ 316°C (2.0, 2.5, and 3.2 gpm @ 600°F), respectively. There was no sign of leak rate increase during the first hour of testing.

After the three tests were completed, the flaw was photographed. The original EDM notch, which was torn on each end, showed plastic deformation in the tear zone. The OD flaw length increased from the original length of 4.3 mm (0.18 in.) to about 8 mm (0.4 in.) after testing 170 min. Figure 10 shows close-up views of the left and right ends of the tearing. To determine the cause of the tearing, fractographic examination was performed. Figure 11 shows the fractographic montage for NUANOD.2-1.0. Compared with that of the other EDM specimen (NUANOD.2D), the ligament of NUANOD.2-1.0 is thinner. Figure 12 shows the SEM fractograph for the tip area of the tapered ligament, indicating a typical ductile tearing feature. Figure 13, a higher-magnification view of the designated area in Figure 12 (as a square), clearly shows voids and dimples. However, as shown in Figures 14 and 15, the ligament area away from the tip region clearly showed the crystallographic facets characteristic of fatigue crack growth at low ΔK level, also observed in SGL-900 and NUANOD.2D.

Based on test conditions and results, the observed fractographic results could be explained as follows. Because the first hour of the test did not show increased leak rates, the tearing of the ligament tip region probably occurred during the second hour. The differential-pressure condition of the second test was higher than that of the first hour (9.9 vs 9.1 MPa [1416 vs. 1302 psig]). Therefore, the 9.1-MPa pressure difference during the first hour may not have been enough to initiate a crack from the blunt tip of the EDM notch. The ductile tearing of the EDM notch tip was initiated by the higher pressure difference (9.9 MPa) of the second hour, and the subsequent crack tearing was caused by fatigue at a leak rate of 9.5~12 L/min at 316°C. Because the blowdown facility does not use a pump, the fatigue was very likely caused by water jet/structure interaction. The leak rate of NUANOD.2-1.0 increased more

rapidly than that of NUANOD.2D, presumably because the tapered ligament of NUANOD.2-1.0 was much thinner and the associated crack growth rate was faster than that of NUANOD.2D. Therefore, we conclude that under prototypical normal operating condition of steam generators, a tapered ligament can be fractured by fatigue at a leak rate higher than 9.5 L/min at 316°C (2.5 gpm at 600°F).

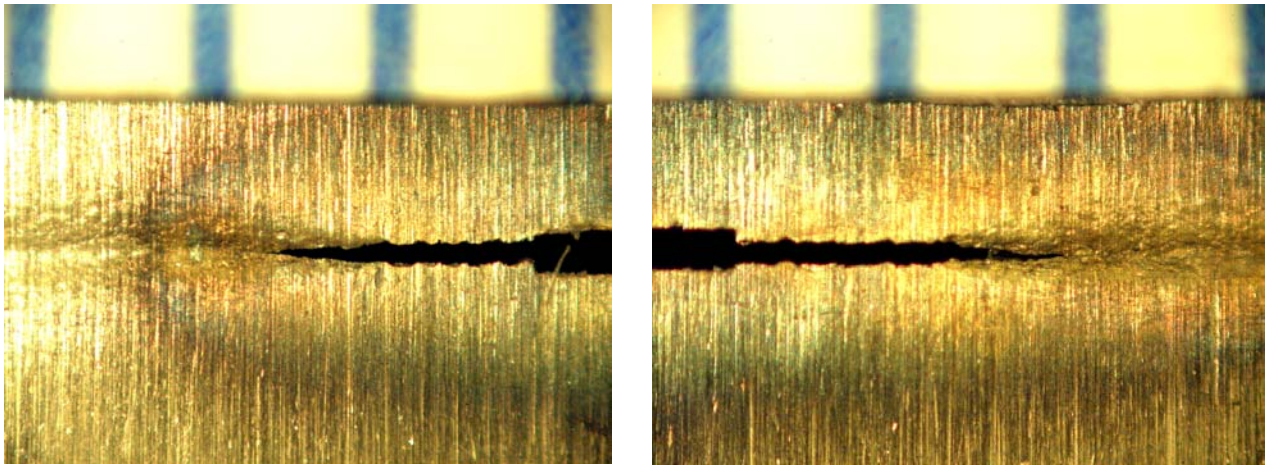

Figure 10. Post-test close-up photograph of (a) left-end and (b) right-end tearing of trapezoidal EDM notch NUANOD.2-1.0 tested at 316°C (600°F) for 170 min [Reproduced from Ref. 13].

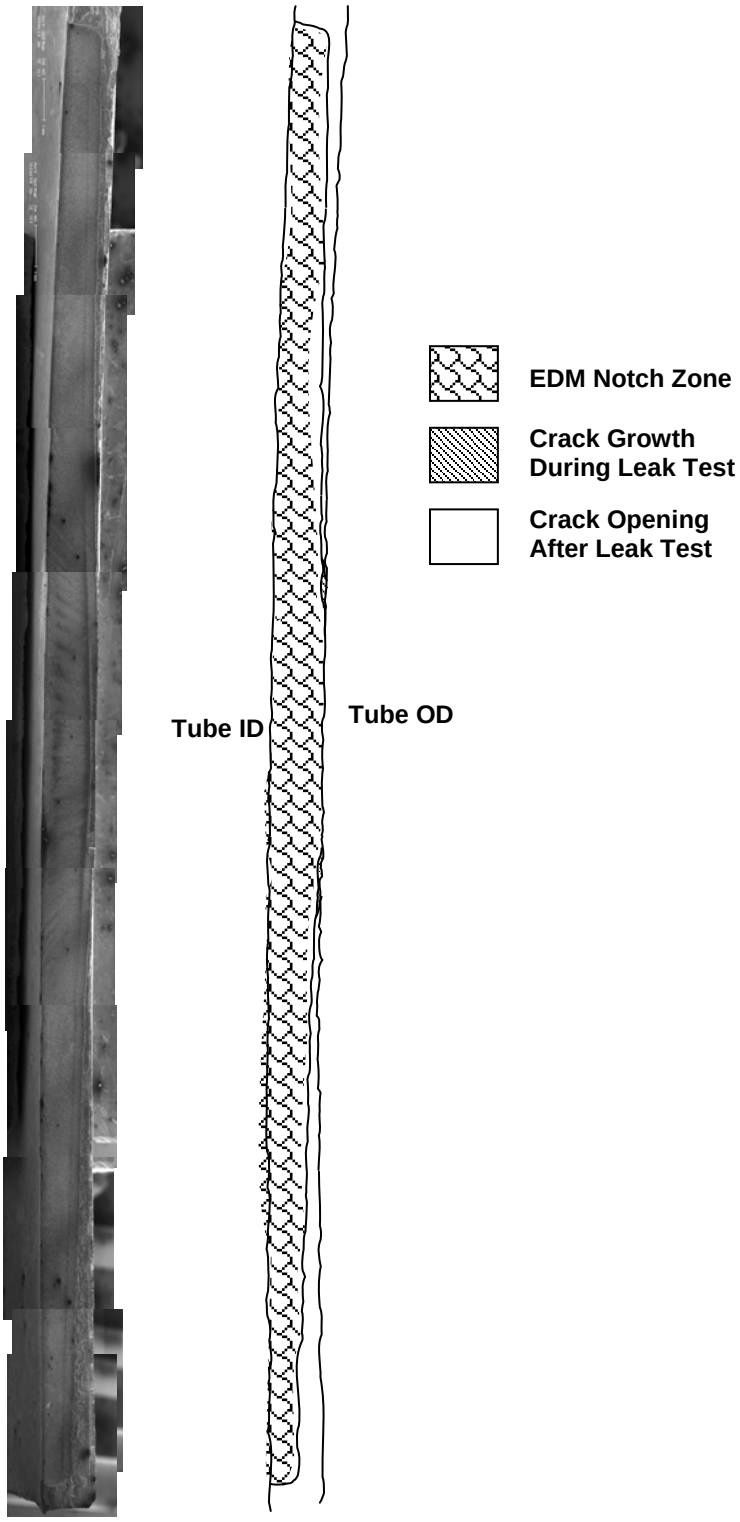

Figure 11. Fractographic montage for EDM notch specimen NUANOD.2-1.0; left and right edges of specimen are tube ID and OD, respectively.

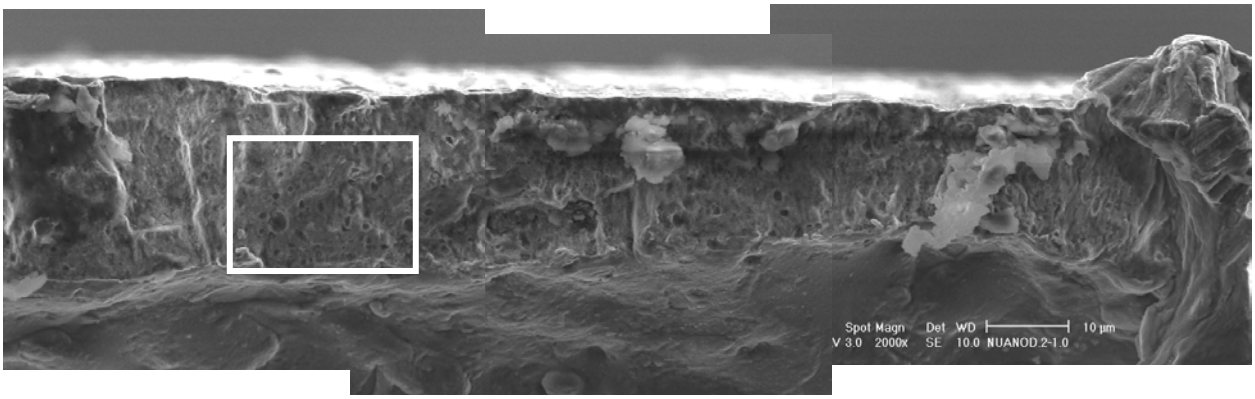

Figure 12. SEM fractograph for tip area of tapered ligament in trapezoidal EDM notch specimen NUANOD.2-1.0, showing voids and dimples.

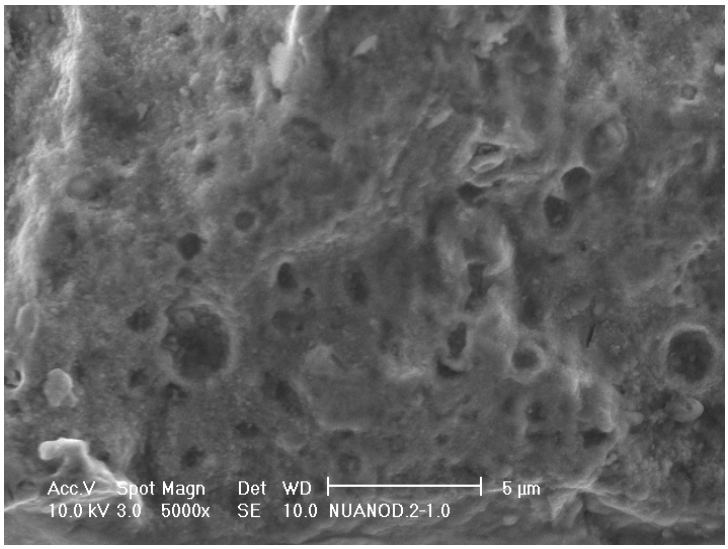

Figure 13.
SEM fractograph with higher magnification of area designated by the box in Figure 12.

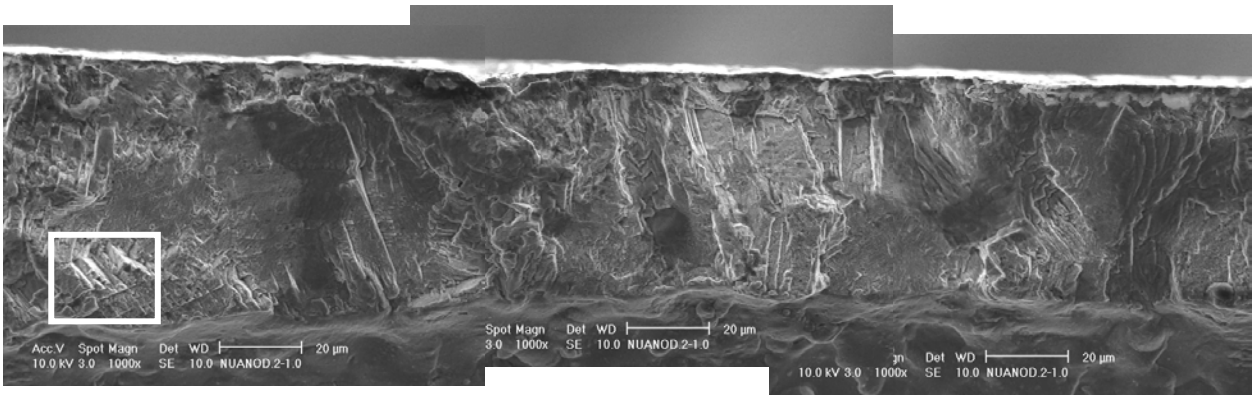

Figure 14. SEM fractograph for area away from the tip area of the tapered ligament in NUANOD.2-1.0, showing crystallographic facets.

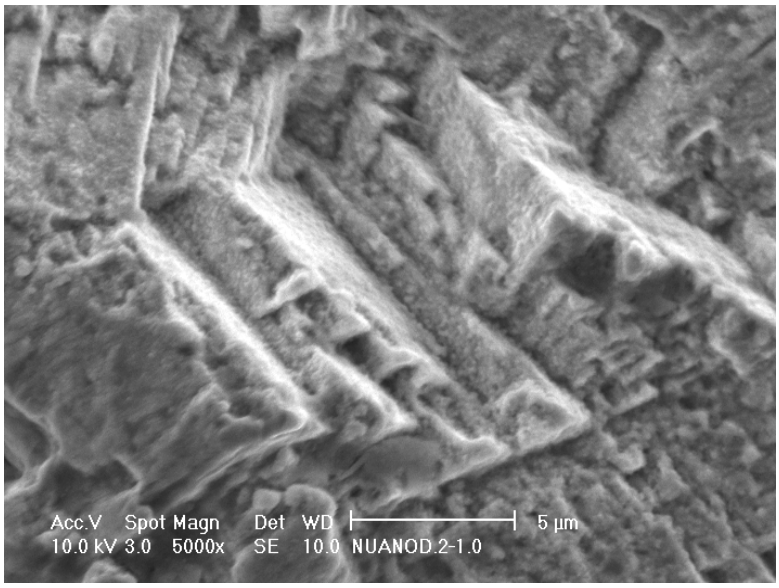

Figure 15.
SEM fractograph with higher magnification of area designated by the box in Figure 14.

Discussion

Results from SCC and EDM-notched specimens discussed in this report are compared in Table 2. Specimen W-2-10 was leak-tested at room temperature for 350 min under a nominally constant pressure of 18.0 MPa (2600 psig), but only a marginal increase in leak rate was observed. On the other hand, Specimen SGL-900 showed a significant increase in leak rate during its 520 min hold at 17.3 MPa (2500 psig). Initial leak rates of the two specimens were almost zero but final leak rates were quite different. This discrepancy may occur because W-2-10 was tested in the blowdown test facility while SGL-900 was tested in the room-temperature high-pressure test facility, which uses a high-pressure triplex pump. This pump caused 100-150 psi peak-to-peak pressure fluctuation, whereas the blowdown test facility imposes no such pressure fluctuations. The pressure fluctuation induced by the pump could be the source of the fatigue crack growth observed in SGL-900. Water leaking from the crack became a jet as the crack opening area became larger. When the leak rate becomes sufficiently high, vibrations due to the water jet/structure interaction could be an additional mechanism for periodic loading. If the water jet does influence the fatigue crack growth of SGL-900, it will be necessary to determine how much of the observed fatigue crack growth was attributable to the water jet and what is the critical leak rate for the water-jet effect to become significant.

SGL-822 was tested in the blowdown facility, as was W-2-10, but the initial TW crack length of SGL-822 was relatively long so that the initial leak rate of this specimen was relatively high. The leak rate of SGL-822 increased rapidly over a short time. Based on fractographic results, the remaining ligaments in the TW crack were fractured by ductile tearing, which caused the rapid increase in leak rate. If we assume that the crack growth of SGL-900 was partially assisted by the jet effect at a higher leak rate (greater than about 2 gpm), it is difficult to explain why SGL-822 did not show any fatigue even though its leak rate was higher than that of SGL-900. One possibility is that the test duration for SGL-822 was too short; if the test were to be continued for more than 35 min, the jet effect might have become significant and fatigue features might have been observed on the fracture surface. Another possible explanation is that because SGL-822 was tested at high temperature without back-pressure on the secondary side, the liquid water flashed to gaseous steam inside the crack or at the exit plane of the crack path, which might cause a less-significant jet effect than in the case of SGL-900 for which there was no phase transformation of steam to water. However, the results of NUANOD.2-1.0, as discussed below, suggest that even under a phase transformation condition of water, the jet could cause the fatigue crack growth. Therefore, it appears likely that the test duration of SGL-822 was too short to activate the jet effect.

As discussed earlier, two specimens (W-2-10 and SGL-822) tested in the blowdown facility did not show any fatigue fracture. The test on the trapezoidal EDM-notched specimen NUANOD.2-1.0 proved that fatigue crack growth could occur under a constant pressure condition like that achievable in the blowdown test facility. Fractographic results for NUANOD.2-1.0 suggest that under a pressure condition similar to that under normal SG operating conditions, the thin ligament can grow by fatigue at a leak rate of around 11 L/min at 316°C (3 gpm at 600°F). Because there was no pressure pulsation in the blowdown facility, the fatigue was most likely caused by the jet/structure interaction. Among all the specimens tested, the test conditions of NUANOD.2-1.0 were closest to the normal operating condition of SGs although the secondary side was mainly filled with steam rather than the two-phase mixture found in the secondary side of actual SGs. The test conditions of SGL-822 were close to those seen in secondary depressurization accidents such as a Main Steam Line Break.

Based on the characterization results for ANL leak rate specimens, it was shown that a tapered thin ligament or a remaining ligament in the TW crack region could be fractured by fatigue during leak testing. For the EDM-notched specimens, this occurred with or without the high-pressure pump. For the SCC specimens, this occurred to date only with the high-pressure pump. Crack growth by fatigue in full-thickness material was evident in some of the

SCC specimens, including SGL-900 and rectangular EDM-notched specimens. But the results from all of these specimens were not unambiguous because pressure pulsations due to both the pump and the jet may have been responsible for the observed crack growth. It is necessary to demonstrate unequivocally that crack growth in full-thickness material can (or cannot) occur by fatigue under a constant pressure condition without a pump such as that used in the blowdown test facility.

Table 2. Comparison of test conditions and results for three SCC and two EDM leak test specimens.

Specimen ID	Pump used?	Pressure Difference, MPa (psi)	Fractography	Leak Rate, L/min (gpm)		Test Duration, min
				Initial	Final	
W-2-10	No	18 (2600) @ RT	Ductile ligament tearing	0.06 (0.015)	0.1 (0.03)	350
SGL-822	No	16.9 (2450) @ 282°C	Ductile ligament tearing	5.7 (1.5)	19 (5.0)	35
SGL-900	Yes	17.3 (2500) @ RT	Fatigue	~0	8.3 (2.2)	520
NUANOD.2D	Yes	6.9 (1000) @ RT	Fatigue	6.1 (1.6)	17 (4.5)	700
NUANOD.2-1.0	No	9.0~9.7 (1300~1400) @ 316°C	Ductile tearing + Fatigue	7.6 (2.0)	12 (3.2)	170

Summary of Characterization Results

- ANL SCC and EDM-notched tube specimens that showed time-dependent leak rate behavior at a constant pressure condition were characterized by fractography to determine the time-dependent crack growth mechanism and by radial metallography to determine the degree of IGA along the main axial stress corrosion crack.
- While some SCC specimens showed typical ductile fracture surface features, others showed distinct crystallographic facets that are typical of fatigue crack growth at low ΔK levels. This implies that time-dependent leak rate growth cannot be attributed to a single mechanism. However, it is noted that all SCC specimens that showed crystallographic facets were tested in the room-temperature high-pressure test facility, which uses a high-pressure triplex pump that causes 690-1000 kPa (100-150 psi) peak-to-peak pressure fluctuations. The specimens that showed ductile fracture were tested in the high-temperature blowdown facility, which maintains a constant pressure condition.
- A trapezoidal EDM-notched specimen NUANOD.2-1.0 tested in the blowdown facility showed crystallographic facets on its fracture surface, which suggests that fatigue crack growth is possible under a constant pressure condition such as that in the blowdown facility.
- Structural vibration, which is very likely the underlying cause for the observed fatigue, appears to be the result of the pressure fluctuation induced by the high-pressure pump and the water jet/tube structure interaction.
- Fractographic results of some SCC specimens indicated that cracks grew by fatigue in full-thickness material. So far, however, this has not been demonstrated to be the case under a constant pressure condition such as that in the blowdown test facility.

- Nonprototypical features of the SCC specimens such as secondary cracks and severe IGA along the dominant axial SCC were observed in the ANL SCC specimens. The effects of these features on time-dependent leak rate growth needs to be evaluated. However, it is difficult to correlate IGA with fatigue crack growth. Both SCC and EDM-notched specimens showed similar fracture surface morphologies, such as crystallographic facets. Because EDM-notched specimens have no IGA, the IGA observed in the SCC specimens is not likely to have contributed to the observed time-dependent leak rate growth.

Evaluation of Fatigue Source

In the previous section, two possible sources for fatigue loading during the ANL leak tests are proposed: pressure fluctuation by the high-pressure pump and vibration by water jet/structure interaction. In this section, earlier reports and literature on the pump pulsation and the water jet/structure interaction are reviewed, and by using an available fatigue crack growth rate equation for Alloy 600, we estimate frequencies and amplitudes of the pressure oscillation induced by the pump and the water jet for earlier ANL test specimens.

Literature Review

Pressure fluctuations in the room-temperature high-pressure test facility under constant pressure conditions have been analyzed.[14] Power spectral density analysis of the pressure transducer signal was carried out for several cases: the pump off (power on), pump on (0 psig) under a "dry" condition (with a bladder/foil, no water jet), pump on (0 psig) under a "wet" condition (with an active water jet), 1000 psig (wet), and 1300 psig (dry and wet). Specimens with EDM notches were used. The frequencies identified for data obtained with various sampling rates are shown in Figure 16. Because the maximum sampling rate was 150 Hz, frequencies higher than 75 Hz could not be identified. The amplitude vs. frequency spectrum for the pressure signal after subtracting out the noise is shown in Figure 17. Four frequencies of 8.42, 16.88, 25.31, and 50.61 Hz were identified. These frequencies are all approximate multiples of the fundamental 8.42 Hz, which is close to an expected frequency of single-piston movement in the high-pressure pump, which has three pistons. The pressure fluctuation amplitudes in both of dry and wet cases appear to be comparable and increase slightly with increasing tube pressure. It is not likely that pressure fluctuation due to the water jet was picked up by the pressure transducer, which has a typical response time of 5 ms (200 Hz). Because the maximum sampling rate was less than the response frequency of the transducer, we need to analyze the pressure fluctuation with a higher sampling rate (>400 Hz) to ensure that the jet frequency did not influence the transducer reading.

Although estimating the crack growth due to pressure oscillations by the pump is relatively straightforward, the same is not true for the water jet effect. The power spectral density of the pressure oscillations by the water jet is not available. An approximate computational fluid dynamics analysis to calculate the jet vortex shedding frequency as a function of the crack length has been conducted,[13] as plotted in Figure 18. The vibration behavior of the water jet is caused by the pressure difference between the water jet and the medium surrounding the jet and initiates from the exit point of the water jet. As discussed in the earlier report[13] and other literature,[15,16] the jet vortex shedding frequencies are described as a nondimensional parameter (the Strouhal number), which is defined as

$$St = \frac{fh}{U}, \tag{1}$$

where f, h, and U denote the jet vortex shedding frequency, plane slit width (or crack width), and jet velocity, respectively. It is expected that for a given geometry, the shedding frequency is proportional to the velocity because characteristic Strouhal numbers are fixed. Sato estimated two characteristic Strouhal numbers for slit nozzles, 0.23 and 0.14.[15] Deo et al. experimentally confirmed these results for the slot nozzle.[16] Slit width and length used in their tests are larger than those of typical SCC or EDM notch specimens. The pressure amplitudes from the water jet effect could not be estimated, whereas the frequency could be. Even if both the jet-induced pressure oscillation frequencies and amplitudes were available, additional analysis, such as dynamic stress analysis (possibly coupled fluid/structural) would be needed to calculate the appropriate crack driving force (ΔK_d) and frequency.

Tamaki et al. experimentally measured the structural vibration by the water jet by using an accelerometer.[17] A nozzle with a 0.5-mm-diameter cylindrical hole was tested, and the hole's length-to-diameter ratio was 20. The accelerometer was mounted near the nozzle tip area and measured the nozzle vibration frequency. Under the differential pressure ranging from 2.0 to 10.0 MPa (290 to 1450 psi), characteristic vibration frequencies were observed between 30-35, 25-30, and 2-3 kHz, independent of pressure condition. The vibration acceleration level appeared to monotonically increase with the differential pressure, but the level increased by less than 10 % from 2.0 to 10.0 MPa. Tamaki et al. insisted that the cavitation shock pressure corresponding to the vibration was caused by cavitation within the nozzle.[17] The nozzle inlet, which had a sharp and square edge similar to a crack in the SG tubing, induced the cavitation. Tamaki et al. also showed that a smoother edge could decrease the cavitation. The measured structural vibration frequencies of a cylindrical nozzle by Tamaki et al. appear to be in the same range of estimated jet frequencies for EDM notch specimens shown in Figure 18. However, the origins of the jet vibration are different; the jet vortex shedding is caused by the pressure difference at the exit of the water jet but the cavitation-induced vibration is caused by the sharp edge of the jet nozzle inlet. Cavitation inside the nozzle depends on geometrical factors such as nozzle length-to-diameter (or width) ratio and sharpness at the nozzle inlet.

It is noted that the independency of the characteristic nozzle vibration frequencies on the differential pressure appears inconsistent with earlier literatures by Sato[15] and Deo et al.[16] Because Sato and Deo et al. insisted that the Strouhal number is constant for a given geometry; this implies that the frequency should increase with increase in the flow velocity (or increase in the differential pressure) as described in Eq. 1. This inconsistency also suggests that the jet vortex shedding and cavitation-induced vibration at the jet nozzle inlet are different phenomena. Sato and Deo et al. used smooth and convergent inlet nozzles, which would minimize the contribution of the cavitation-induced vibration. In the case of leakage through SG tube cracks, it is not clear how much each phenomenon would contribute to the overall water jet effect. At the least, cavitation-induced vibration at the nozzle inlet is expected to contribute because typical stress corrosion cracks would have a sharp edge at the crack inlet. In-situ monitoring of tube vibration by mounting accelerometers near the cracks, as done by Tamaki et al., may be helpful in determining the water jet effect in the cracked SG tubing.

Keskinen[18] reported the dynamic effects of a leak from a circumferential through-crack. The potential for self-excited vibrations due to the water jet was analyzed by the method of conservation of energy. It was assumed that during each vibration cycle the work done by the jet force is consumed by energy losses from structural damping and crack-tip plastic dissipation. Work per cycle was formulated as a function of vibration stress amplitude and compared with each other unit of work. If work done by the jet force is greater than energy consumption by structural damping and crack-tip dissipation, the jet/structure vibration will continue. Numerical results for PWR primary circuit piping suggested that structural damping alone provides sufficient margin against jet-induced instability. This result does not necessarily mean that a jet through an axial or circumferential crack in SG tubing will not cause self-excited vibrations. The structure of SG tubing is much different from that of primary piping. Further evaluation for the SG tubing case by using analytical methods similar to those of Keskinen may be useful.

As discussed above, the range of frequency of the water-jet-induced vibration could be estimated reasonably, but the associated pressure amplitude could not be estimated. Instead, effective pressure amplitudes (using frequency as a parameter) were estimated by back-fitting experimentally measured crack growth data for trapezoidal EDM notches conducted at ANL, as discussed in a later section.

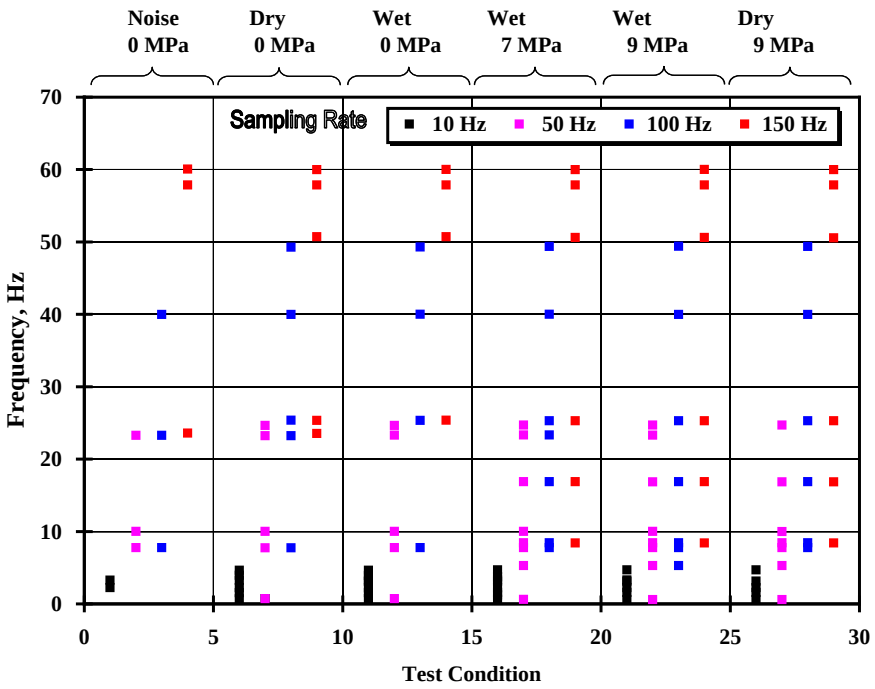

Figure 16. Frequency signals detected by power spectral density analysis of pressure signals under various conditions and sampling rates [Reproduced from Ref. 14].

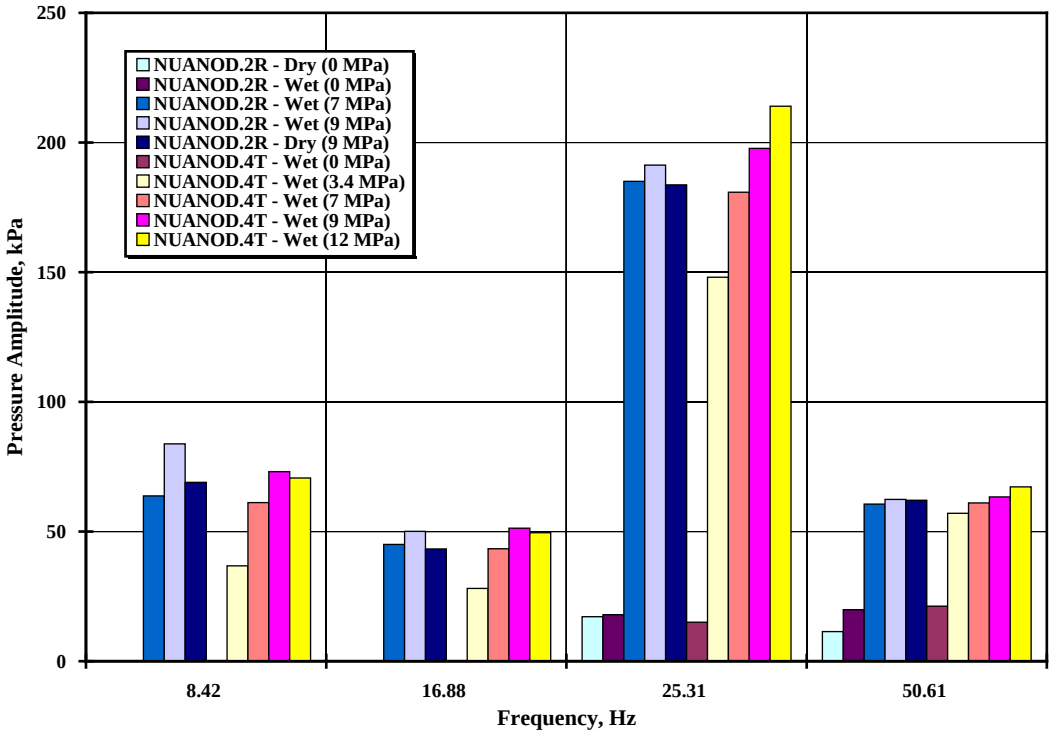

Figure 17. Estimated pressure fluctuation amplitudes as a function of frequency under various test conditions (data sampling rate = 150 Hz) [Reproduced from Ref. 14].

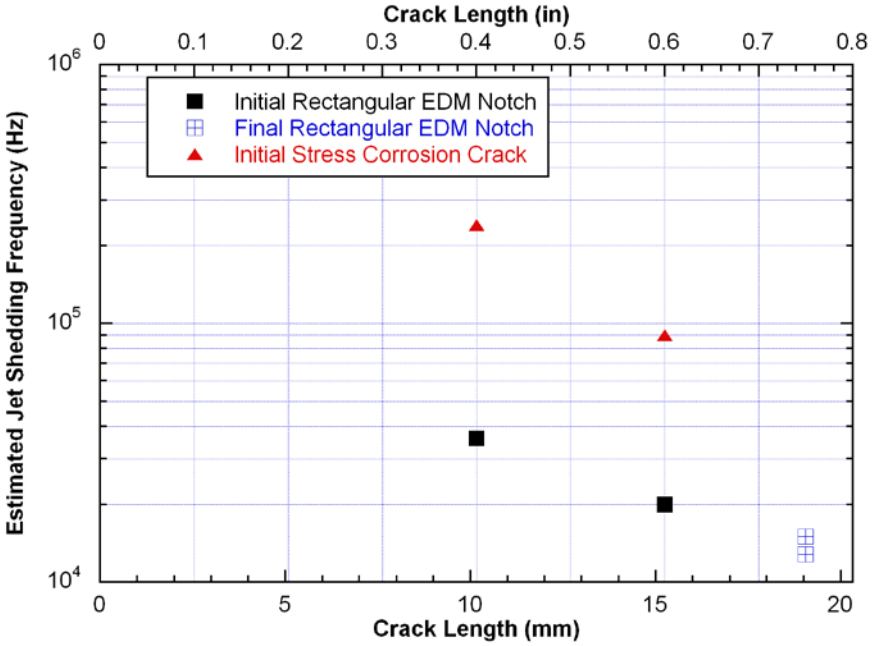

Figure 18. Estimated jet vortex shedding frequencies at 1300 psi steady tube pressure difference (Δp), based on assumed characteristic dimension of 1/4 of crack width [Reproduced from Ref. 13].

Fatigue Crack Growth Rate of Alloy 600

To evaluate the frequency and amplitude induced by the water jet by using the experimental data, a fatigue crack growth rate (CGR) equation for Alloy 600 is needed. An equation proposed by Omesh Chopra et al. was used in this estimation.[19] The CGR (m/cycle) of Alloy 600 in air is expressed as

$$\frac{da}{dN} = C_{A600}\left(1 - 0.82R\right)^{-2.2}\left(\Delta K\right)^{4.1}, \tag{2}$$

where R is stress ratio, ΔK is in $MPa \cdot m^{1/2}$, and constant C_{A600} is given by a third-order polynomial of temperature T (°C) expressed as

$$C_{A600} = 4.835 \times 10^{-14} + \left(1.622 \times 10^{-16}\right)T - \left(1.490 \times 10^{-18}\right)T^2 + \left(4.355 \times 10^{-21}\right)T^3. \tag{3}$$

Eq. 2 is based on test data at various conditions. However, test data performed at a high R (>0.9), which is expected in the fatigue induced by the pump or jet/structure interaction, were not available. Also, the test data used for developing Eq. 2 do not include tests near the fatigue threshold. Therefore, the uncertainty of Eq. 2 at high R and low ΔK should be noted. The K-calibration for trapezoidal cracks was obtained from the correlations developed by Lee et al.[20]

James and Mills[8] experimentally showed the effect of stress ratio on the fatigue crack growth rate of Alloy 600 in high-temperature water. Their results indicated that the fatigue crack growth rate increases exponentially as a function of stress ratio, especially when ΔK is

low. If their test data are extrapolated, the fatigue crack growth rate at R = 0.9 is at least a factor of 10 higher than that at R = 0. Because near-threshold fatigue data of Alloy 600 at low ΔK and high R are not available, to estimate the fatigue crack growth rate observed in the ANL leak test specimens, we need to manipulate the current fatigue data and the fatigue crack growth equation of Alloy 600 measured at low R. To evaluate the accuracy of the equation by Chopra et al. near the fatigue threshold, experimental data near the fatigue threshold of Alloy 600,[11,21] Inconel® 718,[22] 316 SS,[23] and 316LN SS[24] were compared with Eq. 2. Figure 19 shows the fatigue threshold of Alloy 600 in room-temperature air calculated from the equation of Chopra et al. as a function of load ratio R (see solid line in Fig. 19). The stress intensity range ΔK where the fatigue crack growth rate becomes 1E-10 m/cycle was set as a threshold at a given load ratio. Experimental fatigue threshold data for Alloy 600 were limited but at least one data point at R = 0.1 is close to the equation of Chopra et al. The other data point for Alloy 600 at R = 0.8 was acquired in high-temperature water, which usually increases the fatigue crack growth rate and threshold. Therefore, the threshold value of Alloy 600 at R = 0.8 and room-temperature air is expected to be lower than 5.4 MPa√m. The fatigue threshold variation of Inconel® 718 (Ni-base alloy) with load ratio appears similar to that by Chopra et al., especially at higher load ratio. To validate the fatigue CGR equation of Alloy 600 near threshold of Chopra et al., additional experimental data are needed.

As shown in Figure 20, the equation of Chopra et al. does not exhibit a threshold behavior, which means that the fatigue crack growth rate does not drop abruptly to zero near the fatigue threshold. Therefore, it is likely that this equation overestimates the fatigue crack growth rate, especially near or below the fatigue threshold. Again, to validate the fatigue CGR equation at higher R and near threshold, additional experiment should be conducted.

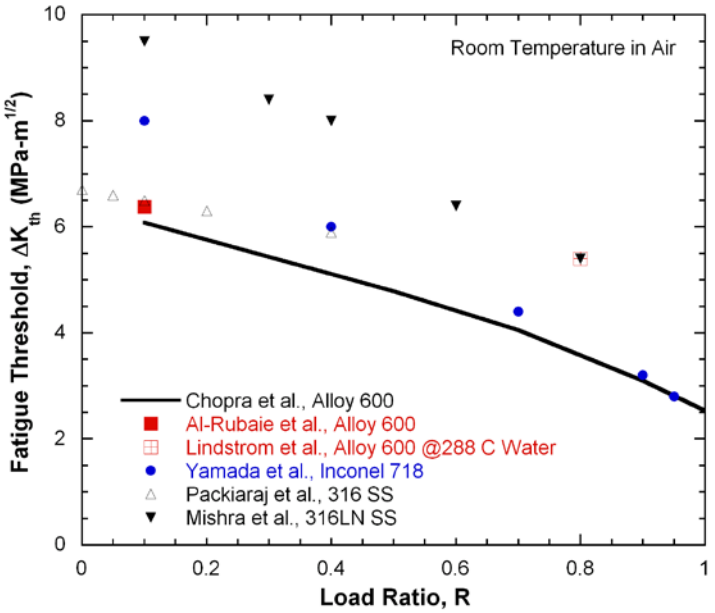

Figure 19.
Fatigue threshold of Alloy 600 at room temperature in air calculated by equation of Chopra et al. as a function of load ratio, R, compared with literature data for Alloy 600, 718, and 316 SS.

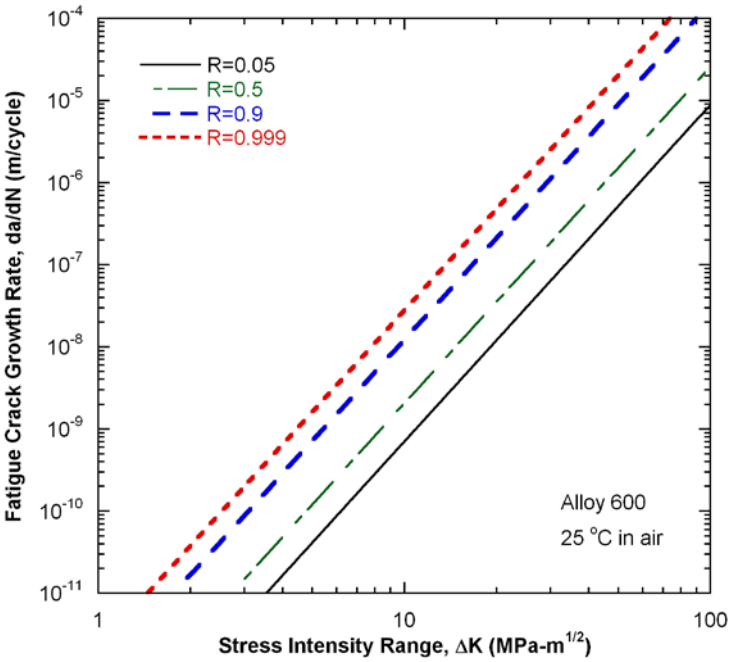

Figure 20.
Fatigue crack growth rate of Alloy 600 by equation of Chopra et al. as a function of stress intensity range and load ratio.

Analysis of Earlier Leak Rate Tests

By using the available fatigue crack growth rate equation shown in Eq. 2, the frequencies and amplitudes from the water jet and from the high-pressure pump were estimated. Measured crack growth data for trapezoidal and rectangular EDM notch specimens were used. The fatigue CGR in crack growth per cycle like that of Eq. 2 can be converted into crack growth per unit of time if the fatigue loading frequency is known. The water jet frequency was deduced by back-fitting the measured crack growth data.

Trapezoidal EDM Notch Specimen

All axial trapezoidal EDM notch specimens evaluated in this section were initially ~5 mm (~0.2 in.) and ~25 mm (~1.0 in.) long at OD and ID, respectively. Figure 21 shows estimated OD crack length variation with time for Specimen NUANOD.2F compared with measured data. The test with NUANOD.2F is composed of two stages: dry and wet. During the dry stage, leakage through the notch was prevented by inserting a bladder and foil into the specimen. During the wet stage, the bladder and foil were removed so that the water jet was activated. Frequency and amplitude of the pressure oscillation due to the pump was estimated from the dry stage data. The estimated pressure oscillation amplitude and the frequency by the pump are 855 kPa (124 psi) peak-to-peak and 50 Hz. Based on the power spectral analysis results (see Fig. 17), 25 Hz is the major frequency, but to keep the estimated pressure oscillation level within the observed range (690-1000 kPa [100-150 psi] peak-to-peak) 50 Hz was selected instead. These values were used as representative values for other trapezoidal EDM notch specimens.

From the wet stage data, contribution of the water jet was estimated. The frequency of the pressure oscillations due to the water jet was set at 40 kHz, as shown in Fig. 18. The average crack length during the wet stage was about 12 mm, which corresponds to a frequency of ~40 kHz. The estimated amplitude by the water jet is 69 kPa (10 psi) peak-to-peak. As shown in Fig. 21, pump oscillation alone (see the solid line denoted as “Full Dry Condition”) could cause significant crack growth during the test. This suggests that at least in the NUANOD.2F test the pump-induced pressure oscillations could make a major contribution to fatigue. Figures 22 and 23 show estimated OD crack length variation with time for NUANOD.2A and NUANOD.2D, respectively, which except for the operating pressure (i.e., 7 MPa vs. 9 MPa [1000 psig vs. 1300 psig]), were identical to the values for Specimen NUANOD.2F. It is apparent that the water jet contributed significantly to the crack growth in these specimens. Although operating pressure has an effect on pressure oscillation due to the pump, the same amplitude and frequency (50 Hz and 855 kPa [124 psi]) were used for these calculations.

The frequency for the jet/structure interaction was set at the same value as in NUANOD.2F, i.e., 40 kHz, because the crack lengths during the tests were similar. The amplitudes for the jet-induced pressure oscillations for NUANOD.2A and NUANOD.2D, calculated from a back fit to the measured data, were 110 kPa (16 psi) and 130 kPa (19 psi) peak-to-peak, respectively, slightly higher than that estimated for NUANOD.2F. As indicated in Figure 23, the crack growth history for NUANOD.2D could also be fitted with the jet oscillation amplitude of 160 kPa (23 psi) instead of 130 kPa (19 psi), provided the pump oscillation amplitude was decreased from 855 to 570 kPa (124 to 82 psi). The estimated jet oscillation amplitudes for trapezoidal specimens are lower than those calculated for the rectangular EDM-notched specimens (to be discussed later).

The amplitude and frequency (855 kPa [124 psi] and 50 Hz) for the pump pressure oscillation estimated from NUANOD.2F under the dry condition appear representative and applicable to other trapezoidal EDM-notch specimens. In a similar fashion, the pressure oscillations due to the water jet, estimated to be in the range of 69 to 130 kPa (10 to 19 psi)

peak-to-peak at a frequency of 40 kHz, appear to be applicable to other trapezoidal EDM-notch specimens.

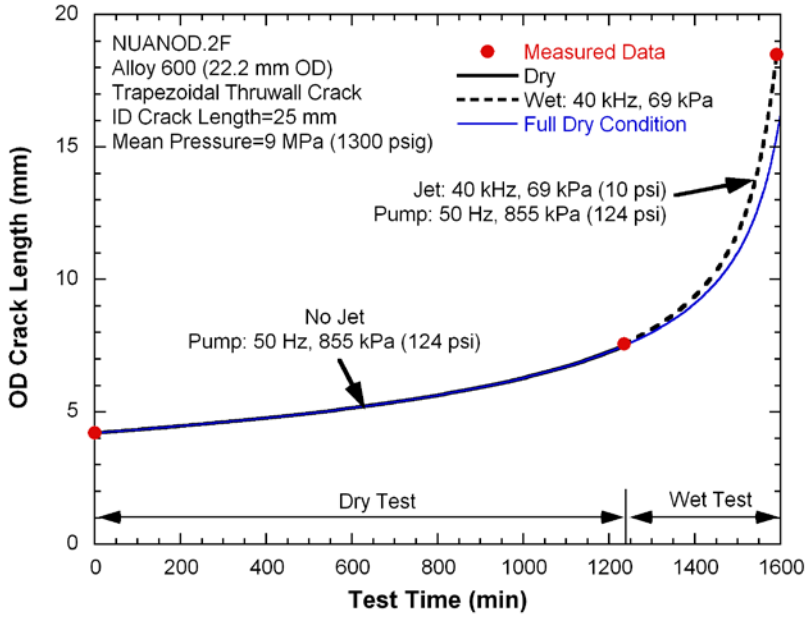

Figure 21.
Estimated OD crack length as a function of test time for specimen NUANOD.2F. compared with measured data.

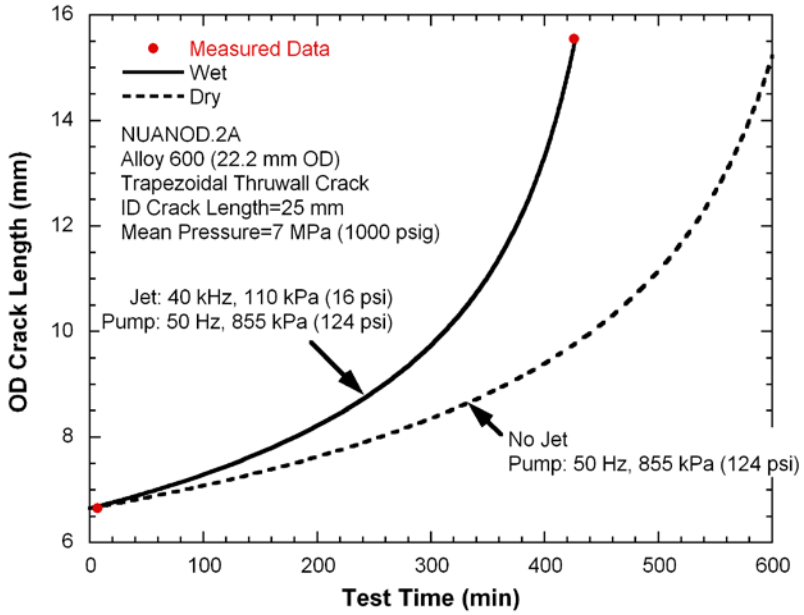

Figure 22.
Estimated OD crack length as a function of test time for the specimen NUANOD.2A compared with measured data.

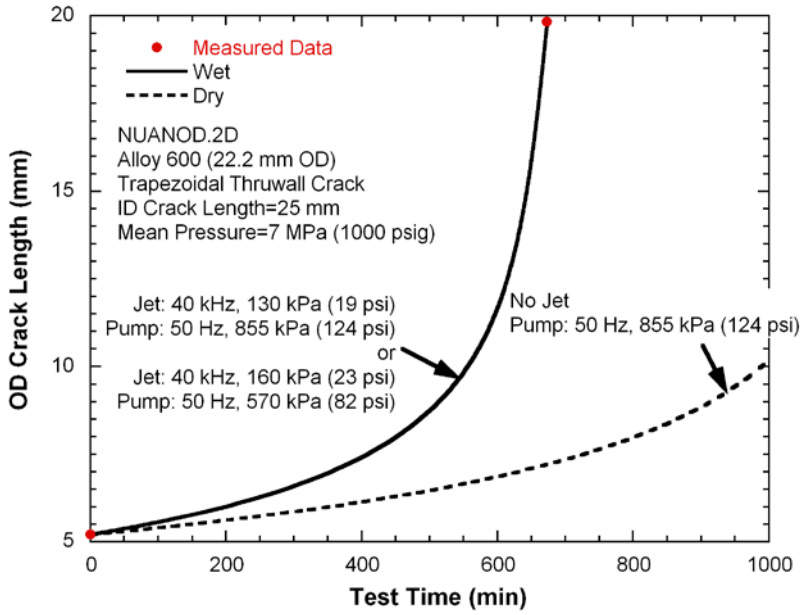

Figure 23.
Estimated OD crack length as a function of test time for specimen NUANOD.2D, compared with measured data.

Rectangular EDM Notch Specimen

Earlier test data with rectangular EDM-notched specimens were also evaluated. Figure 24 shows estimated crack length variation for the specimen NUANOD.4R compared with measured data. This specimen was tested at three different stages: wet test at 12 MPa (1700 psig), wet test at 9 MPa (1300 psig), and dry test at 9 MPa (1300 psig). First, the amplitude and frequency for the pump oscillation were estimated from the dry test data at 9 MPa (1300 psig) (test time: 2580-2890 min) to be 570 kPa (82 psi) peak-to-peak and 50 Hz, respectively. Although the operating pressure in NUANOD.4R was similar to those in trapezoidal EDM-notched specimens, the estimated pump-induced pressure oscillation was smaller. It is not likely that the difference in notch geometry (i.e., rectangular vs. trapezoidal) affects pump oscillation. This discrepancy needs to be evaluated by conducting additional tests.

Oscillation due to the jet in the wet test at 9 MPa (1300 psig) was then calculated by a back-fit to the measured data using the estimated pump-induced pressure oscillations of 570 kPa (82 psi) peak-to-peak at 50 Hz. The calculated pressure oscillation by the jet was 240 kPa (35 psi) peak-to-peak at 20 kHz. A pressure amplitude of 240 kPa (35 psi) was applied again in the wet test at 12 MPa (1700 psig) but the jet frequency was set at 40 kHz because the crack length was shorter. Although the jet oscillation can vary with pressure condition, it is not expected to vary significantly between 9 to 12 MPa (1300 and 1700 psig). However, with the revised jet effect parameters (40 kHz/240 kPa [35 psi]), pump pressure oscillation had to be reevaluated at 12 MPa (1700 psig) to fit the measured data, and the new value of the pump pressure amplitude was 1240 kPa (180 psi) peak-to-peak, significantly higher than the 570 kPa (82 psi) calculated for the 9 MPa (1300 psig) system pressure earlier. Although the pump pressure oscillation amplitude tends to increase with the operating pressure, as shown in Fig. 17, the calculated 1240 kPa (180 psi) amplitude is too high when compared with the pressure oscillation measured by a pressure transducer (690-1000 kPa [100-150 psi] peak-to-peak). This indicates that there are uncertainties in the fatigue CGR equation and in the amplitude and frequency of the jet effect used in this estimation.

Figure 25 shows the estimated crack length variation for a rectangular EDM-notched specimen NUANOD.6W compared with measured data. There are two test stages for this specimen: a wet stage at 9 MPa (1300 psig) and a wet stage at 11 MPa (1640 psig). At 9 MPa

(1300 psig), the same pressure oscillation amplitude/frequency due to the pump as those in NUANOD.4R (570 kPa [82 psi] and 50 Hz) were used. The jet frequency was fixed at 20 kHz and the jet oscillation amplitude was determined by a back fit to the crack growth data to be 220 kPa (32 psi) peak-to-peak, which is quite close to that in NUANOD.4R. Measured data showed a large increase in crack growth rate after the increase in pressure from 9 to 11 MPa (1300 to 1640 psig), which could not be predicted by the 1240 kPa (180 psi) oscillation (dotted line) that was derived as the pump oscillation amplitude earlier. This discrepancy between model and measured data may be due partially to the uncertainty of the fatigue CGR model, but may also be due to crack growth by ductile tearing caused by the pressure increase not accounted for in the CGR model. The crack length history during the wet test at 9 MPa (1300 psig) could also be fitted by using a pump pressure oscillation amplitude of 855 kPa (124 psi), and a jet pressure amplitude of 210 kPa (30 psi) peak-to-peak. However, both the 210 and 220 kPa (30 and 32 psi) jet pressure amplitudes are significantly higher than the 69-130 kPa (10-19 psi) calculated for the trapezoidal notch specimens. This discrepancy may be attributed partly to the uncertainties in the fatigue CGR equation and partly to the uncertainties in the stress intensity factor K calibration for trapezoidal and rectangular cracks, but it needs to be verified by additional tests.

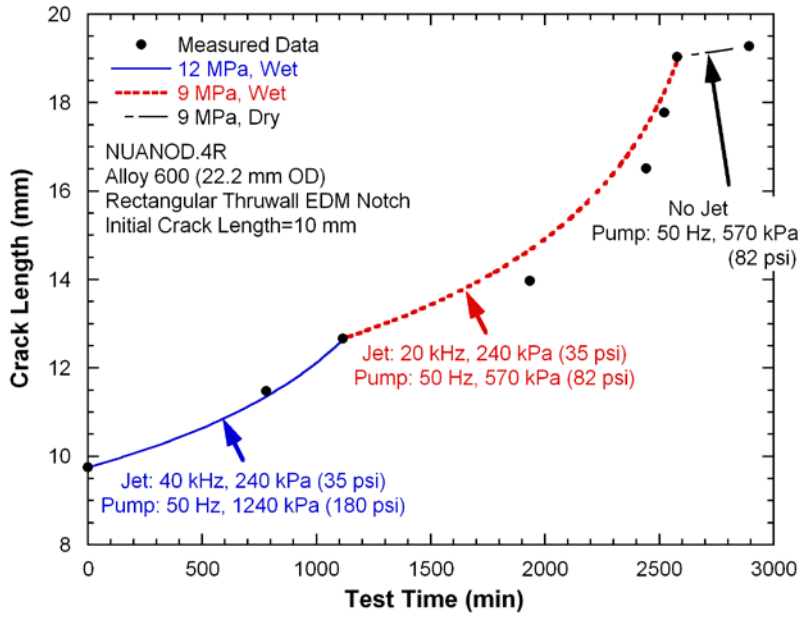

Figure 24.
Estimated crack length as a function of test time for rectangular EDM notch specimen NUANOD.4R, compared with measured data.

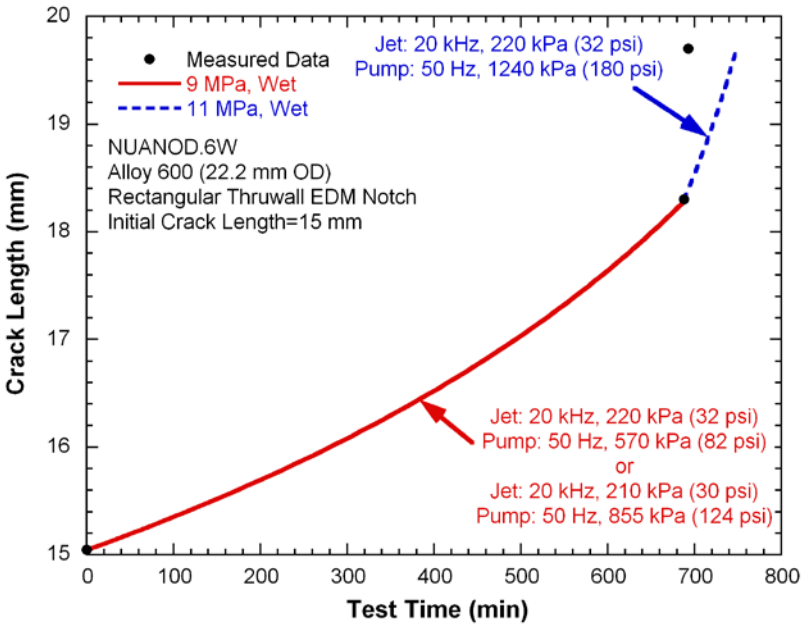

Figure 25.
Estimated crack length as a function of test time for rectangular EDM notch specimen NUANOD.6W, compared with measured data.

Suggested Future Work

Based on the review and evaluation of the ANL time-dependent leak rate test results and earlier literature, several future tests are suggested below.

Fatigue Threshold of Alloy 600

As discussed in an earlier section, the current fatigue crack growth rate equation for Alloy 600 has uncertainties in the lower stress intensity range (near threshold) and a higher load ratio because of limited experimental data. To validate the fatigue crack growth rate equation and evaluate crack growth by jet/structure interaction, fatigue crack growth tests are needed in order to determine the near-threshold growth rate as a function of load ratio, especially at high load ratios.

Leak Tests at Constant Pressure without Pump

In practice, to be conservative a crack deeper than 75% TW is often assumed to be a 100% TW rectangular crack.[20] Therefore, to assure structural integrity of SG tubing, one must determine whether tight TW cracks such as stress corrosion cracks can grow in full-thickness material by the fatigue induced by water jet/structure interaction. Some of the ANL SCC and EDM specimens have shown evidence of fatigue crack growth in full-thickness material but all of these specimens were tested in the high-pressure test facility, which uses a high-pressure pump. Leak tests with rectangular and tight TW cracked specimens should be conducted under a constant pressure condition, like those that can be achieved in the blowdown test facility. Based on the EPRI report,[6] the leak rate range of interest is about 0.2 to 5.7 L/min (0.05 to 1.5 gpm) and the time scale of interest is about 1 to 24 hr.

Because it is impossible to fabricate rectangular TW stress corrosion cracks, the test specimen can be prepared by starting with a part-TW rectangular EDM notch and then growing it TW by oscillating the internal pressure of the tube specimen with a servo-hydraulic machine. An alternative way to fabricate rectangular TW stress corrosion crack specimens is as follows: fabricate axial TW SCC specimens with chemicals and the internal pressurization method and then install the specimens in the room-temperature high-pressure leak test facility and pressurize the specimens to 17.3 MPa (2500 psig). Based on ANL experience, it is expected that the remaining tapered ligaments of the cracks to be fractured by fatigue induced by the pressure oscillation of the high-pressure pump, as well as by the leaking jet. It is also expected that the semi-trapezoidal stress corrosion cracks will grow to become rectangular TW cracks. The leak tests at constant pressure should be performed in the blowdown facility at room temperature, but if a prototypical test condition is required, the test should be performed at high temperature. The differential pressure can be either the normal operating condition or MSLB condition.

Crack Growth Rate Estimation

As described earlier, there are limitations on the test time and leak rate, i.e. <24 hr and <5.7 L/min. Therefore, initial crack length should be limited accordingly; if the crack length is too short, the water jet effect may not be observed within 24 hr, and if the crack length is too long, the leak rate through the crack would be higher than 5.7 L/min. To estimate a reasonable minimum initial crack length, it is necessary to estimate the fatigue crack growth rates of rectangular TW cracks by the water jet as a function of the crack length, recognizing that the estimation may have a large uncertainty. Figure 26 shows the estimated time to 1 mm crack growth of rectangular axial TW cracks at a differential pressure of 17.3 MPa (2500 psig) as a function of the peak-to-peak pressure oscillation by the water jet and for various initial crack lengths. The frequency of pressure oscillations due to the water jet varies with the initial crack length, based on the earlier estimation shown in Fig. 18. The time to 1 mm crack growth for a crack longer than 7.6 mm (0.3 in) could be less than 24 hr if the pressure oscillation by

water jet is greater than ~170 kPa (25 psi) peak-to-peak. Although higher jet oscillation amplitudes can cause faster crack growth, the likelihood of their occurrence at such a high frequency should become increasingly smaller. If the pressure oscillation by the water jet is about 140 kPa (20 psi) or less, the initial crack length may need to be longer than 10.2 mm (0.4 in) in order to observe the water jet effect within 24 hours.

It appears to be possible to observe fatigue crack growth by jet/structure interaction within 24 hours if the initial TW crack length is long enough (≥17.8 mm [0.7 in.]). However, such long cracks may have high leak rates. Because the leak rate range of interest to EPRI is 0.2 to 5.7 L/min (0.05 to 1.5 gpm) to cover the range of main steam line break limits, it is necessary to estimate the leak rate as a function of the initial TW crack length. Figure 27 shows the estimated leak rate for a rectangular axial TW crack in Alloy 600 tubing as a function of crack length. The yield strength of Alloy 600 tubing was assumed as 290 MPa (42 ksi). If the leak rate of interest is less than 5.7 L/min (1.5 gpm), the initial crack length should be less than 10.2 mm (0.4 in). Figure 28 shows the initial or final leak rates of five ANL SCC specimens as a function of corresponding TW crack lengths. Based on fractography of those SCC specimens, all of the SCC cracks became almost rectangular cracks at the end of the leak tests. Therefore, it can be assumed that all SCC cracks were approximately 12-mm-long rectangular TW cracks at the end of the tests. The measured final leak rates corresponding to the 12-mm-long rectangular cracks range from 5.7 to 9.5 L/min (1.5 to 2.5 gpm). Based on these measurement data, the initial rectangular TW crack should be shorter than 12 mm if the leak rate needs to be less than 5.7 L/min (1.5 gpm). But, again it should be noted that there are uncertainties in the fatigue CGR and leak rate models.

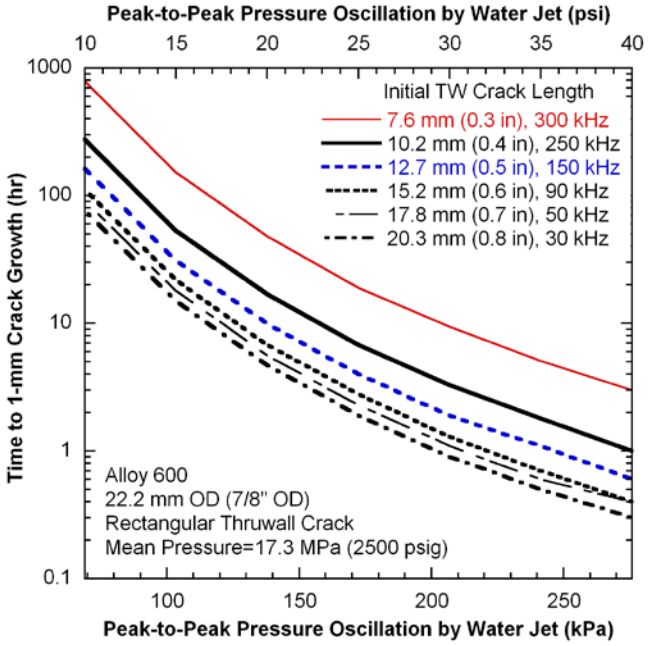

Figure 26.
Estimated time to 1 mm crack growth of rectangular axial TW cracks at 17.3 MPa (2500 psig) as a function of peak-to-peak pressure oscillation by water jet; the jet frequency for each axial TW rectangular crack length was estimated from Figure 18.

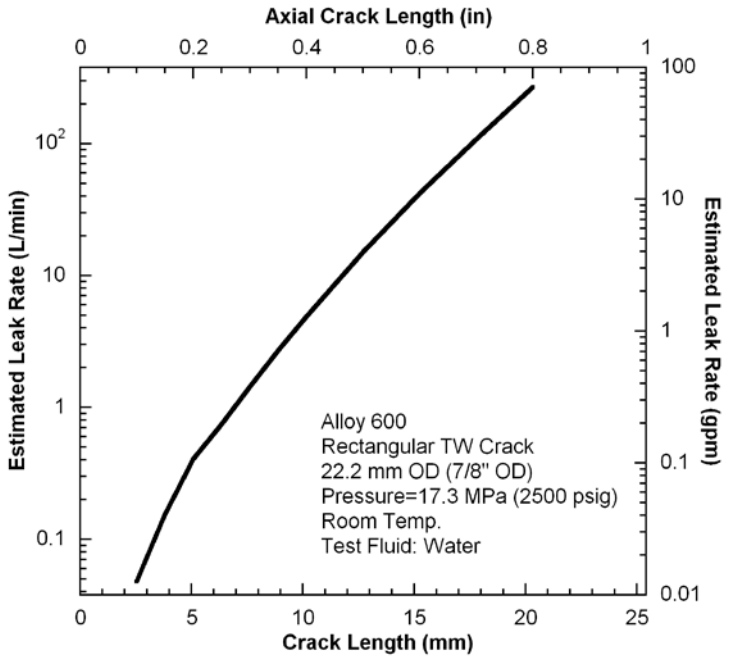

Figure 27.
Estimated leak rate as a function of axial TW crack length for a rectangular TW crack in Alloy 600 tubing; yield strength of Alloy 600 is 290 MPa (42 ksi).

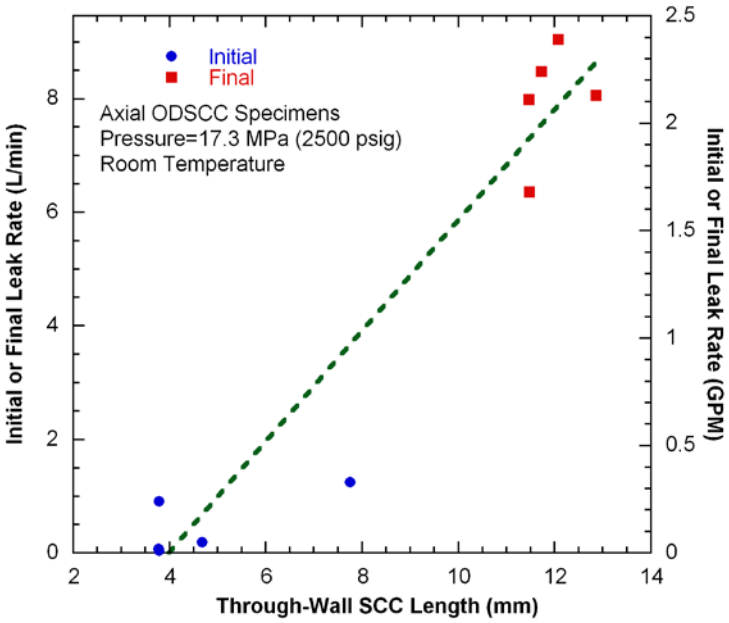

Figure 28.
Initial or final leak rates of five ANL SCC specimens tested at 17.3 MPa (2500 psig) as a function of corresponding TW SCC length [Reprinted with permission from EPRI].[6]

Suggested Test Matrix

If we assume that the test specimens will be made from partially TW EDM notches, a suggested test matrix for time-dependent leak rate tests under constant pressure is shown in Table 3. To keep the initial leak rate less than 1.5 gpm, the initial TW crack length ranges from 5.1 mm (0.2 in.) to 12.7 mm (0.5 in.). A single specimen with an initial EDM notch depth that is deeper than that of the others (40%TW vs. 50%TW) can be tested to determine whether the initial EDM notch depth influences the subsequent leak rate behavior (see Specimen #3 in the test matrix).

Table 3. Suggested test matrix for time-dependent leak rate tests under constant pressure.

Specimen #	Initial TW crack length (mm [in.])	Initial EDM notch depth (%TW)	Comment
1	12.7 [0.5]	40	
2	10.2 [0.4]	40	
3	7.6 [0.3]	50	Effect of EDM notch depth
4	7.6 [0.3]	40	
5	5.1 [0.2]	40	

Submerged and Impinging Water Jet

An earlier ANL leak rate test indicated that crack growth accelerated when the crack area was surrounded by a cylindrical container (as shown in Fig. 29) that induced a submerged and impinging water jet condition. Therefore, to maximize the effect of the jet/structure interaction, leak tests can be performed with the jet impinging on a simulated neighboring tube assembly and under a submerged condition. If a MSLB condition is simulated, the water jet should not be submerged but can impinge on neighboring tubes. In this case, the distance between the jet origin and the impinged object should be considered. For prototypical tests, a SCC tube specimen should be installed in the blowdown test facility and surrounded by a SG tube bundle with the same pitch and geometry as those in actual SGs.

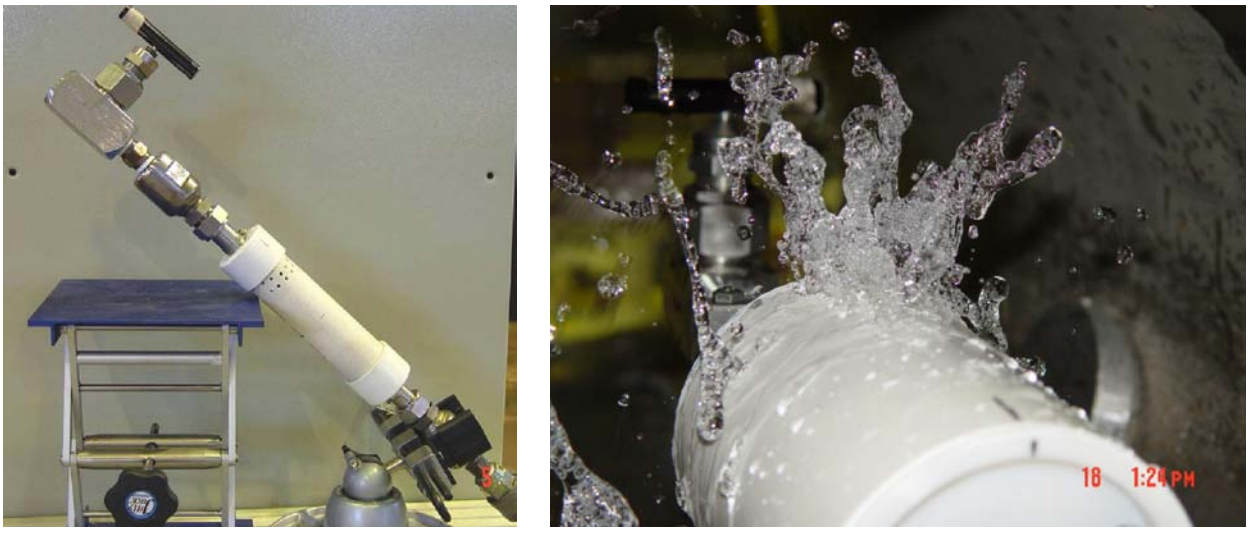

(a) (b)

Figure 29. Photographs showing (a) leak rate test specimen surrounded by a plastic pipe and (b) water coming out of holes on top of the surrounding pipe during a leak rate test.

In-Situ Monitoring of Water Jet

As performed by Tamaki et al.,[17] placing instrumentation close to the flaw with accelerometers could enable measurement of vibration frequencies induced by the water jet. An ultra-high-speed video camera could also be used to record possible jet oscillation.

Summary

Review and evaluation for the ANL leak rate test results at constant pressure are summarized below.

- ANL SCC and EDM-notched tube specimens that have shown time-dependent leak rate behavior under a constant pressure condition were characterized by fractography to determine the time-dependent crack growth mechanisms.
- While some specimens showed typical ductile fracture surface features, others showed distinct crystallographic facets typical of fatigue crack growth at low ΔK level. This implies that time-dependent leak rate growth cannot be attributed to a single mechanism. Some SCC specimens with a high-pressure pump and trapezoidal EDM notch specimens with and without the high-pressure pump indicated fatigue crack growth on their fracture surfaces.
- Structural vibration, which is likely the underlying cause for the observed fatigue, appears to be the result of pressure oscillation induced by the high-pressure pump and the water jet/tube structure interaction.
- The pressure oscillation amplitude and frequency induced by the high-pressure pump could be estimated from the power spectral density analysis for the pressure transducer signals, which corresponded to the frequency of the pump piston stroke.
- The water-jet-induced pressure oscillation could not be estimated from the measured data but had to be estimated from modeling and literatures. There are two possible water-jet-induced vibration phenomena: jet vortex shedding at the jet nozzle exit and cavitation-induced vibration at the jet nozzle inlet. For stress corrosion cracks in SG tubing, both phenomena may contribute to the fatigue crack growth of the SG tubing.
- Calculated results from the crack growth data of trapezoidal and rectangular EDM notch specimens indicated that both the high-pressure pump and the water jet could contribute significantly to fatigue crack growth.

Based on the review and evaluation for the ANL leak rate test results and earlier literatures, possible future work is proposed as follows:

- The currently available fatigue crack growth rate equation of Alloy 600 has uncertainty in the lower stress intensity range and the higher load ratio because of limited experimental data. To validate the fatigue crack growth rate equation and evaluate the crack growth by jet/structure interaction, fatigue tests in the near-threshold regime are needed as a function of load ratio.
- Leak rate tests at constant pressure without the high-pressure pump are needed to determine the critical condition under which the water jet effect becomes significant within 24 hours as a function of crack length. The high-temperature blowdown test facility can provide a stable pressure condition.
- Because an impinging water jet tends to increase the crack growth rate compared to that of a free jet, the test tube specimen should be surrounded by a simulated neighboring SG tube bundle.
- To monitor in-situ the water jet characteristics such as vibration frequencies, accelerometers can be placed close to the crack. An ultra-high-speed video camera could also be used to record possible jet oscillation.

References

1. S. Bakhtiari, K. E. Kasza, D. S. Kupperman, S. Majumdar, J. Y. Park, W. J. Shack, and D. R. Dierks, Second U.S. Nuclear Regulatory Commission International Steam Generator Tube Integrity Research Program: Final Project Summary Report, NUREG/CR-6804, ANL-02/28, U.S. Nuclear Regulatory Commission, Sept. 2003.

2. W. J. Shack, Steam Generator Tube Integrity Program-3 Monthly Progress Report for March 2005, U.S. Nuclear Regulatory Commission, Washington, DC, April 2005.

3. S. S. Hwang, H. P. Kim, J. S. Kim, K. E. Kasza, J. Park, and W. J. Shack, Leak behavior of SCC degraded steam generator tubing of nuclear power plant, *Nucl. Eng. Design* **235** (2005) 2477-2484.

4. S. S. Hwang, C. Nam-gung, J. Park, M. K. Jung, H. P. Kim, and J. S. Kim, Leak Behavior of SCC Degraded SG Tubes at a Constant Pressure, *Key Engineering Materials* **345-346** (2007) 1345-1348.

5. J. Zhao, T. Mo, and D. Nie, The occurrence of room-temperature creep in cracked 304 stainless steel specimens and its effect on crack growth behavior, *Mater. Sci. Eng. A* **483-484** (2008) 572-575.

6. J. Begley, An Evaluation of Time Dependent Leak Rates in Degraded Steam Generator Tubing: Characterization of ANL Leak Rate Specimens, Electric Power Research Institute, Palo Alto, CA: 2008, 1016560.

7. G. F. Pittinato, SEM/TEM Fractography Handbook, Columbus, OH: Metals and Ceramics Information Center, 1975, pp. 39-40.

8. Lee A. James and William J. Mills, "Fatigue-Crack Propagation Behavior of Wrought Alloy 600 and Weld-Deposited EN82H in an Elevated Temperature Aqueous Environment," PVP-Vol. 303, ASME 1995, pp. 21-36.

9. W. J. Mills and L. A. James, "The Fatigue-Crack Propagation Response of Two Nickel-Base Alloys in a Liquid Sodium Environment," *J. Engineering Materials and Technology*, **101** (1979) 205-213.

10. Lee A. James and William J. Mills, "Effect of Heat-Treatment and Heat-To-Heat Variations in the Fatigue-Crack Growth Response of Alloy 718," *Engineering Fracture Mechanics*, **22** (1985) 797-817.

11. K. S. Al-Rubaie, L. B. Godefroid, and J. A.M. Lopes, Statistical modeling of fatigue crack growth rate in Inconel Alloy 600, *Int. J. Fatigue* **29** (2007) 931-940.

12. A. Shyam, S. A. Padula II, S. I. Marras, and W. W. Milligan, Fatigue-Crack-Propagation Thresholds in a Nickel-Base Superalloy at High Frequencies and Temperatures, *Metall. Mater. Trans. A* **33A** (2002) 1949-1962.

13. W. J. Shack, Steam Generator Tube Integrity Program-3 Monthly Progress Report for April 2005, U.S. Nuclear Regulatory Commission, Washington, DC, May 2005.

14. W. J. Shack, Steam Generator Tube Integrity Program-3 Monthly Progress Report for February 2005, U.S. Nuclear Regulatory Commission, Washington, DC, March 2005.

15. H. Sato, The stability and transition of a two-dimensional jet, *J. Fluid Mechanics* **7** (1960) 53-80.

16. R. C. Deo, J. Mi, and G. J. Nathan, The influence of Reynolds number on a plane jet, *Phys. Fluids* **20** (2008) 075108.

17. N. Tamaki, M. Shimizu, K. Nishida, and H. Hiroyasu, Effects of Cavitation and Internal Flow on Atomization of a Liquid Jet, *Atomization and Sprays* **8** (1998) 179-197.

18. R. P. Keskinen, Dynamic Stability of Pipes under Jet Forces from a Circumferential Through-Crack, *J. Pressure Vessel Tech.* **109** (1987) 329-335.

19. O. K. Chopra, W. K. Soppet, and W. J. Shack, Effects of Alloy Chemistry, Cold Work, and Water Chemistry on Corrosion Fatigue and Stress Corrosion Cracking of Nickel Alloys and Welds, NUREG/CR-6721, ANL-01/07, U.S. Nuclear Regulatory Commission, April 2001, pp. 5-7.

20. J. H. Lee, Y. W. Park, H. D. Chung, Y. H. Choi, and S. Majumdar, Investigation on behavior of trapezoidal through-wall cracks under constant pressure loading, *Int. J. Press. Vessels & Piping* **85** (2008) 606-611.

21. R. Lindstrom, P. Lidar, and B. Rosborg, Fatigue Crack Growth Thresholds Measurements in Structural Materials, Fatigue Crack Thresholds, Endurance Limits, and Design, ASTM STP 1372, J. C. Newman, Jr. and R. S. Piascik, eds., American Society for Testing and Materials, West Conshohocken, PA, 2000, pp. 400-410.

22. Y. Yamada and J.C. Newman Jr., Crack closure under high load-ratio conditions for Inconel-718 near threshold behavior, *Eng. Fracture Mech.* **76** (2009) 209-220.

23. C. C. Packiaraj, S. K. Ray, and S. L. Mannan, The influence of crack closure on the positive load ratio (R) dependence of fatigue threshold stress intensity factor range (ΔK_{th}) of AISI 316 stainless steel in air at room temperature, *Int. J. Press. Vessels & Piping* **57** (1994) 65-70.

24. M. P. Mishra, C. C. Packiaraj, S. K. Ray, and S. L. Mannan, Influence of sodium environment and load ratio (R) on fatigue crack growth behavior of a Type 316 LN stainless steel at 813 K, *Int. J. Press. Vessels & Piping* **70** (1997) 77-82.